Dynamo action produced by an anisotropic rotor immersed in an electrically conducting medium at rest

Franck Plunian, Thierry Alboussière

Dynamo action produced by an anisotropic rotor immersed in an electrically conducting medium at rest

Franck Plunian [*]
Université Grenoble Alpes, Université Savoie Mont Blanc, Centre National de la Recherche Scientifique, IRD, Université Gustave Eiffel, ISTerre, Grenoble 38000, France

Thierry Alboussière [†]
Université Lyon 1, ENS de Lyon, Centre National de la Recherche Scientifique, Laboratoire de Géologie de Lyon, Lyon 69622, France

(Received 28 April 2023; accepted 18 October 2023; published 17 November 2023)

It is shown that the rotational motion of a cylindrical rotor immersed in an electro-conducting medium at rest can produce a dynamo effect, provided that the electrical conductivity or magnetic permeability of the rotor is anisotropic. Results are reported for three pairs of rotor materials: copper/kapton, iron/tin, and μ-metal/tin. The value of using such an anisotropic rotor in liquid metal such as sodium or galinstan for a laboratory dynamo experiment is clearly demonstrated.

DOI: 10.1103/PhysRevFluids.8.113702

I. INTRODUCTION

Dynamo action is known as the spontaneous generation of a magnetic field by the motion of an electrically conducting material. This process is responsible for the magnetic field present in most astrophysical objects, often linked to differential rotation and strong turbulence [1,2], whatever the origin of the motion, convection, precession, or tides [3].

Despite the success of several past achievements, the experimental demonstration of the dynamo effect still remains a technical challenge, especially if a liquid metal is used [4–6]. The main difficulties are the injection of a sufficiently large amount of kinetic energy into the flow, a flow geometry suitable for dynamo action, and a sufficiently electrically conducting fluid. Liquid sodium is generally used, with a number of well-known constraints: It has a high melting temperature (100 °C), is combustible in contact with air, and is explosive in contact with water.

Another solution is to use solid electrical conductors, as in the experiment of Lowes and Wilkinson [7,8] which consisted in two rotating cylinders in cylindrical cavities inside a block made of the same material, the electrical contact being ensured by a thin layer of mercury. Mercury has the advantage of being liquid at room temperature, but nowadays galinstan, an alloy of gallium, indium, and tin, also liquid at room temperature, is preferred, although new difficulties may arise, related to the oxidation of galinstan in air, as reported in [9,10] in an experimental reproduction of the disk dynamo of Bullard [11].

Recently, a new dynamo experiment, called Fury, was built and has been running for over two years now [12]. It is based on the differential rotation between two coaxial cylinders, a rotor and a stator, both with anisotropic electrical conductivity. The experiment is therefore mainly solid, except for a small gap between the two cylinders which is filled with galinstan. On the sides of the

[*]franck.plunian@univ-grenoble-alpes.fr
[†]thierry.alboussiere@ens-lyon.fr

cylinders, a silver coating was used to ensure good electrical contact with the galinstan. In addition, dilute hydrochloric acid is applied to the top surface of galinstan to prevent oxidation. The dynamo threshold is relatively low, corresponding to a rotation frequency of the rotor, of about 25 Hz. This experiment has the advantage of being of small size (17 cm in diameter by 21 cm in height), easily reproducible and relatively inexpensive.

This also opens up new possibilities, for example by replacing the external stator with a liquid metal such as sodium. Again, the dynamo would be triggered by the differential rotation between the anisotropic rotor and the conducting fluid. It could be argued that the use of such an anisotropic rotor to start the dynamo is rather far from natural dynamos. It is true that with this solution the dynamo would not be generated by the fluid's own motion. However, it is still a self-excited dynamo in liquid metal, without the aid of a magnet or an electric battery, and presumably more efficient than mechanical forcing by a propeller. In addition, it has a potential wealth of nonlinear behavior due to the feedback of Laplace-Lorentz forces on the dynamo, as in [13]. From the theoretical point of view, the main difference with the fully anisotropic case [14,15] is that the external medium which is now liquid is necessarily isotropic. In this new configuration, several questions emerge: Is the dynamo possible and how does it change the dynamo threshold? An additional option is also interesting, if the anisotropy of the rotor is based on magnetic permeability instead of electrical conductivity, as in [16].

The general formulation of the problem is presented in Sec. II, followed by the expressions of the boundary conditions in Sec. III. The solutions are derived in Sec. IV, leading to a dispersion relation and then to an analytical expression of the dynamo threshold. The results are presented in Sec. V, for three types of rotors. In practice, to design an anisotropic rotor, a combination of two different materials is required. The combinations copper/kapton, iron/tin, and μ-metal/tin will be considered, corresponding to a strong anisotropy of electrical conductivity in the first case, and to a strong anisotropy of magnetic permeability for the last two. For each type of rotor, two external liquid metals will be considered: galinstan and liquid sodium.

II. GENERAL FORMULATION

We consider the solid body rotation of a cylindrical rotor of radius R, surrounded by a medium at rest. The velocity field is then given by

$$\boldsymbol{U} = r\tilde{\Omega}\boldsymbol{e}_\theta, \quad \text{with} \quad \tilde{\Omega} = \begin{cases} \Omega, & \text{for } r < R \\ 0, & \text{for } r > R \end{cases}, \tag{1}$$

where Ω is the rotor's angular velocity, and $(\boldsymbol{e}_r, \boldsymbol{e}_\theta, \boldsymbol{e}_z)$ and (r, θ, z) are unit basis vectors and coordinates in cylindrical geometry. The external fluid is considered to be approximately at rest, at least for some time, with Stewartson boundary layers at the walls of the cylinder, sufficiently thin to be ignored.

The electrical conductivity and magnetic permeability of the rotor are taken as anisotropic, which means that they take different values depending on the direction considered. Although we are interested in an external medium whose electrical conductivity and magnetic permeability are isotropic, it is mathematically more convenient to consider first the general case where both the rotor and the external medium are anisotropic, and to return to the case of an isotropic external medium only at the end.

Following Ruderman and Ruzmaikin [17], we define the electrical conductivity and the magnetic permeability by $\sigma^\parallel$ and $\mu^\parallel$ in a given direction $\boldsymbol{q}$, and by $\sigma^\perp$ and $\mu^\perp$ in the directions perpendicular to $\boldsymbol{q}$, where $\boldsymbol{q}$ is a unit vector. In the direction parallel to $\boldsymbol{q}$, Ohm's law and the relation between $\boldsymbol{H}$ and $\boldsymbol{B}$ are written in the form $\boldsymbol{J}\cdot\boldsymbol{q} = \sigma^\parallel(\boldsymbol{E}\cdot\boldsymbol{q})$ and $\boldsymbol{B}\cdot\boldsymbol{q} = \mu^\parallel(\boldsymbol{H}\cdot\boldsymbol{q})$, while in the directions perpendicular to $\boldsymbol{q}$, they are written as $\boldsymbol{J} - (\boldsymbol{J}\cdot\boldsymbol{q})\boldsymbol{q} = \sigma^\perp[\boldsymbol{E} - (\boldsymbol{E}\cdot\boldsymbol{q})\boldsymbol{q}]$ and $\boldsymbol{B} - (\boldsymbol{B}\cdot\boldsymbol{q})\boldsymbol{q} = \mu^\perp[\boldsymbol{H} - (\boldsymbol{H}\cdot\boldsymbol{q})\boldsymbol{q}]$. This leads to two symmetric tensors, $[\sigma_{ij}]$ for the electrical

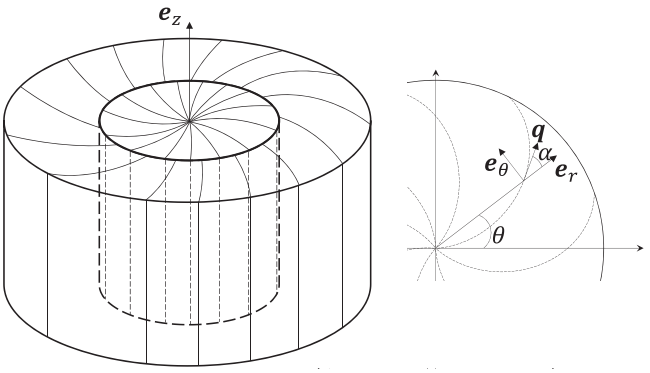

FIG. 1. Left: Perspective view of the inner rotor and outer stator for the fully anisotropic case. The spiral surfaces correspond to the favored directions of the electric current (resp. magnetic field) for an anisotropic electrical conductivity (resp. magnetic permeability). These surfaces are perpendicular to $\boldsymbol{q}$ which is shown on the right, seen from above.

conductivity and $[\mu_{ij}]$ for the magnetic permeability, defined by

$$[\sigma_{ij}] = \sigma^{\perp}\delta_{ij} + (\sigma^{\parallel} - \sigma^{\perp})q_i q_j, \quad [\mu_{ij}] = \mu^{\perp}\delta_{ij} + (\mu^{\parallel} - \mu^{\perp})q_i q_j. \tag{2}$$

In order to have a formulation that encompasses both the rotor and the external medium, we introduce the subscripts "in" for the rotor and "out" for the external medium, such that in (2) the two tensors depend on $\sigma^{\perp}_{\rm in}$, $\sigma^{\parallel}_{\rm in}$, $\mu^{\perp}_{\rm in}$, and $\mu^{\parallel}_{\rm in}$ for the rotor and $\sigma^{\perp}_{\rm out}$, $\sigma^{\parallel}_{\rm out}$, $\mu^{\perp}_{\rm out}$, and $\mu^{\parallel}_{\rm out}$ for the external medium. Anticipating a renormalization of the electrical conductivity and magnetic permeability by $\sigma^{\perp}_{\rm in}$ and $\mu^{\perp}_{\rm in}$, it is then useful to rewrite these tensors as follows:

$$[\sigma_{ij}] = \sigma^{\perp}_{\rm in}\,\tilde{\varphi}_\sigma\left(\delta_{ij} - \frac{\tilde{\sigma}}{1+\tilde{\sigma}}q_i q_j\right), \quad [\mu_{ij}] = \mu^{\perp}_{\rm in}\,\tilde{\varphi}_\mu\left(\delta_{ij} - \frac{\tilde{\mu}}{1+\tilde{\mu}}q_i q_j\right), \tag{3}$$

with

$$\tilde{\varphi}_\sigma = \begin{cases} 1 \\ \varphi_\sigma \end{cases}, \quad \tilde{\sigma} = \begin{cases} \sigma_{\rm in} \\ \sigma_{\rm out} \end{cases}, \quad \tilde{\varphi}_\mu = \begin{cases} 1 \\ \varphi_\mu \end{cases}, \quad \tilde{\mu} = \begin{cases} \mu_{\rm in} & \text{for} \quad r < R \\ \mu_{\rm out} & \text{for} \quad r > R \end{cases}, \tag{4}$$

$$\varphi_\sigma = \frac{\sigma^{\perp}_{\rm out}}{\sigma^{\perp}_{\rm in}}, \quad \sigma_{\rm in} = \frac{\sigma^{\perp}_{\rm in}}{\sigma^{\parallel}_{\rm in}} - 1, \quad \sigma_{\rm out} = \frac{\sigma^{\perp}_{\rm out}}{\sigma^{\parallel}_{\rm out}} - 1, \tag{5}$$

$$\varphi_\mu = \frac{\mu^{\perp}_{\rm out}}{\mu^{\perp}_{\rm in}}, \quad \mu_{\rm in} = \frac{\mu^{\perp}_{\rm in}}{\mu^{\parallel}_{\rm in}} - 1, \quad \mu_{\rm out} = \frac{\mu^{\perp}_{\rm out}}{\mu^{\parallel}_{\rm out}} - 1, \tag{6}$$

the case of an isotropic external medium corresponding to $\sigma_{\rm out} = \mu_{\rm out} = 0$.

As in Plunian and Alboussière [15,16,18], we choose $\boldsymbol{q}$ as a unit vector in the horizontal plane defined by

$$\boldsymbol{q} = c\,\boldsymbol{e}_r + s\,\boldsymbol{e}_\theta, \tag{7}$$

where $c = \cos\alpha$ and $s = \sin\alpha$, with α a prescribed angle. The vector $\boldsymbol{q}$ is tangential to logarithmic spirals in the horizontal plane $(\boldsymbol{e}_r, \boldsymbol{e}_\theta)$ as shown in Fig. 1.

In the magnetohydrodynamic approximation, Maxwell's equations and Ohm's law take the following forms:

$$\boldsymbol{H} = [\mu_{ij}]^{-1}\boldsymbol{B}, \tag{8a}$$

$$\nabla \cdot \boldsymbol{B} = 0, \tag{8b}$$

$$\boldsymbol{J} = \nabla \times \boldsymbol{H}, \tag{8c}$$

$$\partial_t \boldsymbol{B} = -\nabla \times \boldsymbol{E}, \tag{8d}$$

$$\boldsymbol{J} = [\sigma_{ij}](\boldsymbol{E} + \boldsymbol{U} \times \boldsymbol{B}), \tag{8e}$$

leading to the equation for the magnetic induction $\boldsymbol{B}$:

$$\partial_t \boldsymbol{B} = \nabla \times (\boldsymbol{U} \times \boldsymbol{B}) - \nabla \times \{[\sigma_{ij}]^{-1} \nabla \times ([\mu_{ij}]^{-1} \boldsymbol{B})\}, \tag{9}$$

where

$$[\sigma_{ij}]^{-1} = (\tilde{\varphi}_\sigma \sigma_{\text{in}}^{\perp})^{-1}(\delta_{ij} + \tilde{\sigma} q_i q_j), \tag{10a}$$

$$[\mu_{ij}]^{-1} = (\tilde{\varphi}_\mu \mu_{\text{in}}^{\perp})^{-1}(\delta_{ij} + \tilde{\mu} q_i q_j). \tag{10b}$$

Equations (10) are derived from (3) knowing that, for any unit vector $\boldsymbol{q}$ and any scalar quantity $X \neq -1$, we have

$$\left[\delta_{ij} - \frac{X}{1+X} q_i q_j\right]^{-1} = \delta_{ij} + X q_i q_j. \tag{11}$$

Since the velocity is stationary and independent of z, and as we are considering only axisymmetric solutions, because they are the least dissipative ones and then likely to be dominant at the dynamo onset, we look for a magnetic induction in the form

$$\boldsymbol{B} = \boldsymbol{B}(r) \exp(\gamma t + ikz), \tag{12}$$

where $\boldsymbol{B}(r)$ is the axisymmetric magnetic mode at vertical wave number k. In (12) a positive value of the real part of the magnetic growth rate γ is the signature of dynamo action. The dynamo threshold that we will seek corresponds to $\text{Re}\{\gamma\} = 0$.

Replacing (1) and (12) in (9), and after some algebra (see Appendix A), one obtains the following equations for $B_r(r)$ and $B_\theta(r)$:

$$\tilde{\gamma} B_r = -(\sigma_{\text{in}}^{\perp} \mu_{\text{in}}^{\perp})^{-1}[\tilde{\mu} c^2 k^2 B_r + (1 + \tilde{\sigma} s^2) D_k(B_r) - cs(\tilde{\sigma} - \tilde{\mu}) k^2 B_\theta], \tag{13a}$$

$$\tilde{\gamma} B_\theta = -(\sigma_{\text{in}}^{\perp} \mu_{\text{in}}^{\perp})^{-1}[\tilde{\sigma} c^2 k^2 B_\theta + (1 + \tilde{\mu} s^2) D_k(B_\theta) - cs(\tilde{\sigma} - \tilde{\mu}) D_k(B_r)], \tag{13b}$$

where

$$\tilde{\gamma} = \tilde{\varphi}_\sigma \tilde{\varphi}_\mu \gamma = \begin{cases} \gamma, & \text{for } r < R \\ \varphi_\sigma \varphi_\mu \gamma, & \text{for } r > R \end{cases} \tag{14}$$

and

$$D_k(X) = k^2 X - \partial_r \left(\frac{1}{r} \partial_r (rX) \right). \tag{15}$$

III. BOUNDARY CONDITIONS AND RENORMALIZATION

The system of equations (13) must be completed by the appropriate boundary conditions for $r = 0$ and $r \to \infty$,

$$B_r(r=0) = B_\theta(r=0) = \lim_{r\to\infty} B_r = \lim_{r\to\infty} B_\theta = 0, \tag{16}$$

and by the continuity across $r = R$ of the normal component of $\boldsymbol{B}$, and of the tangential components of $\boldsymbol{H}$ and $\boldsymbol{E}$:

$$[B_r]_{r=R^-}^{r=R^+} = [H_\theta]_{r=R^-}^{r=R^+} = [H_z]_{r=R^-}^{r=R^+} = [E_\theta]_{r=R^-}^{r=R^+} = [E_z]_{r=R^-}^{r=R^+} = 0, \tag{17}$$

where $[X]_{r=R^-}^{r=R^+} = X(R^+) - X(R^-)$.

From (8a) and (10b), the magnetic field $\boldsymbol{H}$ takes the form

$$\boldsymbol{H} = \left(\tilde{\varphi}_\mu \mu_{\rm in}^{\perp}\right)^{-1} \begin{pmatrix} (1+\tilde{\mu}c^2)B_r + \tilde{\mu}csB_\theta \\ \tilde{\mu}csB_r + (1+\tilde{\mu}s^2)B_\theta \\ B_z \end{pmatrix}, \tag{18}$$

with, from (8b),

$$B_z = ik^{-1}\left(\frac{B_r}{r} + \frac{\partial B_r}{\partial r}\right). \tag{19}$$

Then the first three conditions in (17) can be rewritten as

$$B_r(R^+) = B_r(R^-), \tag{20}$$

$$\varphi_\mu^{-1}[\mu_{\rm out}csB_r(R^+) + (1+\mu_{\rm out}s^2)B_\theta(R^+)] = \mu_{\rm in}csB_r(R^-) + (1+\mu_{\rm in}s^2)B_\theta(R^-), \tag{21}$$

$$\varphi_\mu^{-1}\left(\frac{B_r(R^+)}{R} + \frac{\partial B_r}{\partial r}(R^+)\right) = \frac{B_r(R^-)}{R} + \frac{\partial B_r}{\partial r}(R^-). \tag{22}$$

From (8d) we have $E_\theta = -ik^{-1}\gamma B_r$, implying that the first and fourth conditions in (17) are redundant. As for the last boundary condition in (17), using (8e) we have

$$J_z = \sigma_{\rm in}^{\perp}\tilde{\varphi}_\sigma(E_z - \tilde{\Omega}rB_r) \tag{23}$$

with $\tilde{\Omega}$ defined in (1), leading to

$$\varphi_\sigma^{-1}J_z(R^+) - J_z(R^-) = \sigma_{\rm in}^{\perp}\Omega RB_r(R^-). \tag{24}$$

Renormalizing the distance and time by R and $\mu_{\rm in}^{\perp}\sigma_{\rm in}^{\perp}R^2$, and the current density $\boldsymbol{J}$ by $(\mu_{\rm in}^{\perp}R)^{-1}$, corresponds to replacing R, $\sigma_{\rm in}^{\perp}$, and $\mu_{\rm in}^{\perp}$ by unity in the system (13a) and in the boundary conditions (16), (20)–(22), and (24). Then the absolute value of the dimensionless angular velocity $|\Omega|$ corresponds to the magnetic Reynolds number.

IV. RESOLUTION

The resolution of the system (13) follows the same line as in [18]. Introducing

$$k_{\tilde{\sigma}} = k\left(\frac{1+\tilde{\sigma}+\tilde{\gamma}/k^2}{1+\tilde{\sigma}s^2}\right)^{1/2}, \quad k_{\tilde{\mu}} = k\left(\frac{1+\tilde{\mu}+\tilde{\gamma}/k^2}{1+\tilde{\mu}s^2}\right)^{1/2}, \tag{25}$$

and with the help of the identity

$$D_{k_1}(X) = D_{k_2}(X) + \left(k_1^2 - k_2^2\right)X, \tag{26}$$

the system (13) takes the following form:

$$(1+\tilde{\sigma}s^2)D_{k_{\tilde{\sigma}}}(B_r) = (\tilde{\sigma}-\tilde{\mu})ck^2(cB_r + sB_\theta), \tag{27a}$$

$$(1+\tilde{\mu}s^2)D_{k_{\tilde{\mu}}}(B_\theta) = (\tilde{\sigma}-\tilde{\mu})c(sD_k(B_r) - ck^2B_\theta). \tag{27b}$$

Then we can show that (see Appendix B)

$$D_{k_{\tilde{\mu}}}(cB_r + sB_\theta) = D_{k_{\tilde{\sigma}}}(sD_k(B_r) - ck^2B_\theta) = 0. \tag{28}$$

Then, using (28) and (27) leads to

$$\left(D_{k_{\tilde{\mu}}} \circ D_{k_{\tilde{\sigma}}}\right)(B_r) = \left(D_{k_{\tilde{\sigma}}} \circ D_{k_{\tilde{\mu}}}\right)(B_\theta) = 0. \tag{29}$$

The two operators $D_{k_{\tilde{\sigma}}}$ and $D_{k_{\tilde{\mu}}}$ being commutative, B_r and B_θ satisfy the same linear differential equation of fourth order. As the solution of $D_\nu(X) = 0$ is a linear combination of $I_1(\nu r)$ and $K_1(\nu r)$, where I_1 and K_1 are first and second kind modified Bessel functions of order 1, the solutions of

(29) are a linear combination of $I_1(k_{\tilde{\sigma}}r)$, $K_1(k_{\tilde{\sigma}}r)$, $I_1(k_{\tilde{\mu}}r)$, and $K_1(k_{\tilde{\mu}}r)$. Applying the boundary conditions (16), B_r and B_θ can be written in the following form:

$$B_r = \begin{cases} r < 1, & -s\left(\lambda_{\sigma_{\rm in}} \frac{I_1(k_{\sigma_{\rm in}} r)}{I_1(k_{\sigma_{\rm in}})} + \lambda_{\mu_{\rm in}} \frac{I_1(k_{\mu_{\rm in}} r)}{I_1(k_{\mu_{\rm in}})}\right) \\ r > 1, & -s\left(\lambda_{\sigma_{\rm out}} \frac{K_1(k_{\sigma_{\rm out}} r)}{K_1(k_{\sigma_{\rm out}})} + \lambda_{\mu_{\rm out}} \frac{K_1(k_{\mu_{\rm out}} r)}{K_1(k_{\mu_{\rm out}})}\right) \end{cases}, \tag{30}$$

$$B_\theta = \begin{cases} r < 1, & c\left(\lambda_{\sigma_{\rm in}} \frac{I_1(k_{\sigma_{\rm in}} r)}{I_1(k_{\sigma_{\rm in}})} + \frac{\mu_{\rm in} s^2 + \frac{\gamma s^2}{c^2 k^2}}{1+\mu_{\rm in} s^2} \lambda_{\mu_{\rm in}} \frac{I_1(k_{\mu_{\rm in}} r)}{I_1(k_{\mu_{\rm in}})}\right) \\ r > 1, & c\left(\lambda_{\sigma_{\rm out}} \frac{K_1(k_{\sigma_{\rm out}} r)}{K_1(k_{\sigma_{\rm out}})} + \frac{\mu_{\rm out} s^2 + \varphi_\sigma \varphi_\mu \frac{\gamma s^2}{c^2 k^2}}{1+\mu_{\rm out} s^2} \lambda_{\mu_{\rm out}} \frac{K_1(k_{\mu_{\rm out}} r)}{K_1(k_{\mu_{\rm out}})}\right) \end{cases}, \tag{31}$$

where B_θ has been obtained from B_r by replacing (30) in (27a), $D_{k_\sigma}(B_r)$ being derived in Appendix C.

The boundary conditions (20), (21), and (22) lead to [see Appendix D for the derivation of (34)]

$$\lambda_{\sigma_{\rm in}} + \lambda_{\mu_{\rm in}} = \lambda_{\sigma_{\rm out}} + \lambda_{\mu_{\rm out}}, \tag{32}$$

$$\lambda_{\sigma_{\rm in}} + \frac{\gamma s^2}{c^2 k^2} \lambda_{\mu_{\rm in}} = \varphi_\mu^{-1} \left(\lambda_{\sigma_{\rm out}} + \varphi_\sigma \varphi_\mu \frac{\gamma s^2}{c^2 k^2} \lambda_{\mu_{\rm out}}\right), \tag{33}$$

$$\lambda_{\sigma_{\rm in}} k_{\sigma_{\rm in}} \frac{I_0(k_{\sigma_{\rm in}})}{I_1(k_{\sigma_{\rm in}})} + \lambda_{\mu_{\rm in}} k_{\mu_{\rm in}} \frac{I_0(k_{\mu_{\rm in}})}{I_1(k_{\mu_{\rm in}})} = -\varphi_\mu^{-1} \left(\lambda_{\sigma_{\rm out}} k_{\sigma_{\rm out}} \frac{K_0(k_{\sigma_{\rm out}})}{K_1(k_{\sigma_{\rm out}})} + \lambda_{\mu_{\rm out}} k_{\mu_{\rm out}} \frac{K_0(k_{\mu_{\rm out}})}{K_1(k_{\mu_{\rm out}})}\right). \tag{34}$$

Finally, to apply the last boundary condition (24) we need to calculate the z component of the current density, that is derived by replacing B_r and B_θ given by (30) and (31), in (8a) and (8c), leading to (see Appendix E)

$$\boldsymbol{J}_z = \begin{cases} r < 1, & c\left[k_{\sigma_{\rm in}} \lambda_{\sigma_{\rm in}} \frac{I_0(k_{\sigma_{\rm in}} r)}{I_1(k_{\sigma_{\rm in}})} + \frac{\gamma s^2}{c^2 k^2} \lambda_{\mu_{\rm in}} k_{\mu_{\rm in}} \frac{I_0(k_{\mu_{\rm in}} r)}{I_1(k_{\mu_{\rm in}})}\right] \\ r > 1, & -c\varphi_\mu^{-1}\left[k_{\sigma_{\rm out}} \lambda_{\sigma_{\rm out}} \frac{K_0(k_{\sigma_{\rm out}} r)}{K_1(k_{\sigma_{\rm out}})} + \frac{\gamma s^2}{c^2 k^2} \varphi_\sigma \varphi_\mu \lambda_{\mu_{\rm out}} k_{\mu_{\rm out}} \frac{K_0(k_{\mu_{\rm out}} r)}{K_1(k_{\mu_{\rm out}})}\right] \end{cases}. \tag{35}$$

Replacing (30) and (35) in (24) leads to

$$\begin{aligned} \frac{s}{c}\left(\lambda_{\sigma_{\rm in}} + \lambda_{\mu_{\rm in}}\right)\Omega = {} & \lambda_{\sigma_{\rm in}} k_{\sigma_{\rm in}} \frac{I_0(k_{\sigma_{\rm in}})}{I_1(k_{\sigma_{\rm in}})} + \frac{\gamma s^2}{c^2 k^2} \lambda_{\mu_{\rm in}} k_{\mu_{\rm in}} \frac{I_0(k_{\mu_{\rm in}})}{I_1(k_{\mu_{\rm in}})} \\ & + \varphi_\sigma^{-1} \varphi_\mu^{-1} \left(\lambda_{\sigma_{\rm out}} k_{\sigma_{\rm out}} \frac{K_0(k_{\sigma_{\rm out}})}{K_1(k_{\sigma_{\rm out}})} + \frac{\gamma s^2}{c^2 k^2} \varphi_\sigma \varphi_\mu \lambda_{\mu_{\rm out}} k_{\mu_{\rm out}} \frac{K_0(k_{\mu_{\rm out}})}{K_1(k_{\mu_{\rm out}})}\right). \end{aligned} \tag{36}$$

A dispersion relation can then been derived, writing that the determinant of the system composed of the four equations (32), (33), (34), and (36) and the four unknowns $\lambda_{\sigma_{\rm in}}$, $\lambda_{\sigma_{\rm out}}$, $\lambda_{\mu_{\rm in}}$, and $\lambda_{\mu_{\rm out}}$ must be equal to zero. In two previous papers [16,18] dispersion relations for the case in which $\sigma_{\rm in} = \sigma_{\rm out}$, $\mu_{\rm in} = \mu_{\rm out}$, and $\varphi_\sigma = \varphi_\mu = 1$ have been derived. They correspond to the fully anisotropic case, i.e., when the external medium has the same anisotropy as the rotor. In [16] the conjugated effect of electrical conductivity and magnetic permeability on the dynamo threshold ($\gamma = 0$) was studied, while in [18] it is the asymptotic behavior of the growth rate γ, in the limit of large $|\Omega|$, which was studied, leading to a new type of dynamo called furious. Now we derive the dynamo threshold in the general case $\sigma_{\rm in} \neq \sigma_{\rm out}$, $\mu_{\rm in} \neq \mu_{\rm out}$, $\varphi_\sigma \neq 1$, and $\varphi_\mu \neq 1$.

Introducing the functions

$$\Phi(x) = xI_0(x)/I_1(x), \quad \Psi(x) = xK_0(x)/K_1(x), \tag{37}$$

and after some algebra, the following dispersion relation is found:

$$\Omega^c = -\frac{c}{s}\frac{\left[\Phi\left(k_{\sigma_{\text{in}}}\right)+\varphi_\sigma^{-1}\Psi\left(k_{\sigma_{\text{out}}}\right)\right]\left[\Phi\left(k_{\mu_{\text{in}}}\right)+\varphi_\mu^{-1}\Psi\left(k_{\mu_{\text{out}}}\right)\right]}{\Phi\left(k_{\sigma_{\text{in}}}\right)+\Psi\left(k_{\sigma_{\text{out}}}\right)-\Phi\left(k_{\mu_{\text{in}}}\right)-\Psi\left(k_{\mu_{\text{out}}}\right)}, \tag{38}$$

where $k_{\sigma_{\text{in}}}$, $k_{\sigma_{\text{out}}}$, $k_{\mu_{\text{in}}}$, and $k_{\mu_{\text{out}}}$ are taken from (25) for $\gamma = 0$. The dispersion relation given by (38), together with (5), (6), and (25), covers all possible cases, isotropy or anisotropy of the inner or outer part, and any inner to outer ratio of electrical conductivity or magnetic permeability. The only assumption is the geometry of the anisotropy, if any, in logarithmic spiral shape of angle α. We note that for $\varphi_\sigma = \varphi_\mu = 1$, $\sigma_{\text{in}} = \sigma_{\text{out}}$, and $\mu_{\text{in}} = \mu_{\text{out}}$ the dispersion relation (38) is identical to the one in [16], and to the one in [18] with $\gamma = 0$. If in addition $\mu_{\text{in}} = \mu_{\text{out}} = 0$, corresponding to an isotropic permeability everywhere, then the dispersion relation of [15] can also been recovered. From (38), we see that exchanging σ and μ corresponds to changing Ω^c in $-\Omega^c$, as already demonstrated by [19,20] for isotropic electrical conductivity and isotropic magnetic permeability, and also verified by Plunian and Alboussière [16,18] for the fully anisotropic case.

V. RESULTS

As explained in the Introduction, here we restrict our analysis to an external medium with isotropic electromagnetic properties, $\sigma_{\text{out}}^{\perp} = \sigma_{\text{out}}^{\parallel}$ and $\mu_{\text{out}}^{\perp} = \mu_{\text{out}}^{\parallel}$, which implies that $\sigma_{\text{out}} = \mu_{\text{out}} = 0$. Looking for the dynamo threshold $\gamma = 0$ implies in addition that $k_{\sigma_{\text{out}}} = k_{\mu_{\text{out}}} = k$. Then, (38) simplifies into

$$\Omega^c = -\frac{c}{s}\frac{\left[\Phi\left(k_{\sigma_{\text{in}}}\right)+\varphi_\sigma^{-1}\Psi(k)\right]\left[\Phi\left(k_{\mu_{\text{in}}}\right)+\varphi_\mu^{-1}\Psi(k)\right]}{\Phi\left(k_{\sigma_{\text{in}}}\right)-\Phi\left(k_{\mu_{\text{in}}}\right)}. \tag{39}$$

From (39) we immediately see that if $\varphi_\sigma \ll 1$ or $\varphi_\mu \ll 1$, then $|\Omega^c| \gg 1$, suggesting that an external medium with an electrical conductivity or magnetic permeability much lower than the rotor's will prevent the dynamo from occurring. However, we must keep in mind that Ω^c is a dimensionless quantity. For a dimensional rotor frequency, this statement, while still relevant, is not necessarily so binding as shown below. Eventually, it is shown in Appendix H that $\Omega^c \propto k^{-2}$ for $k \to 0$, and $\Omega^c \propto k$ for $k \to \infty$, implying the existence of a value of k for which $|\Omega^c|$ reaches a minimum.

From (39), for given values of $\sigma_{\text{in}}^{\perp}$ and $\mu_{\text{in}}^{\perp}$, the results depend on four parameters, σ_{in}, μ_{in}, φ_σ, and φ_μ, the first two characterizing the anisotropy of the rotor, the last two characterizing the electrical and magnetic properties of the external medium with respect to those of the rotor. The results also depend on α, which controls the geometry of the anisotropy. In Sec. V A, we take $\alpha = 0.16\pi$, essentially because it is the value taken in the Fury experiment [12], corresponding to the minimum dynamo threshold of the fully anisotropic case, obtained for $\sigma_{\text{in}} \gg 1$, $\mu_{\text{in}} = 0$, and $\varphi_\sigma = \varphi_\mu = 1$ [15]. Then for such value $\alpha = 0.16\pi$, a minimum dynamo threshold with respect to k is found. In Sec. V B, the value of α is varied in order to find the minimum dynamo threshold with respect to both k and α.

With, again, experimental applications in mind, we consider a rotor which is composed of two materials, the first one with electrical conductivity $\sigma_{\text{in}}^{\perp}$ and magnetic permeability $\mu_{\text{in}}^{\perp}$, the second one with electrical conductivity $\sigma_{\text{in}}^{\parallel}$ and magnetic permeability $\mu_{\text{in}}^{\parallel}$. One way to build an anisotropic rotor is then to alternate vertical layers of the two materials, bent in logarithmic spirals perpendicular to $\boldsymbol{q}$. Of course the rotor is not homogeneous anymore or axisymmetric. However, provided the number of layers is sufficiently large, the previous homogeneous, axisymmetric, and anisotropic model is still a good approximation. In the Fury experiment [12], a cylindrical piece of copper was split over its entire height into narrow spirals into which kapton sheets were then slid, as shown in Fig. 2. Due to the high resistivity of kapton, electric currents then prefer to flow through the copper spirals, despite the thinness of the kapton sheets, thus mimicking anisotropic electrical conductivity.

As mentioned in Sec. I, three types of rotor are now investigated, copper$^{(\perp)}$/kapton$^{(\parallel)}$ as in [12], but also iron$^{(\perp)}$/tin$^{(\parallel)}$ and μ-metal$^{(\perp)}$/tin$^{(\parallel)}$. The choice of these three pairs of materials is

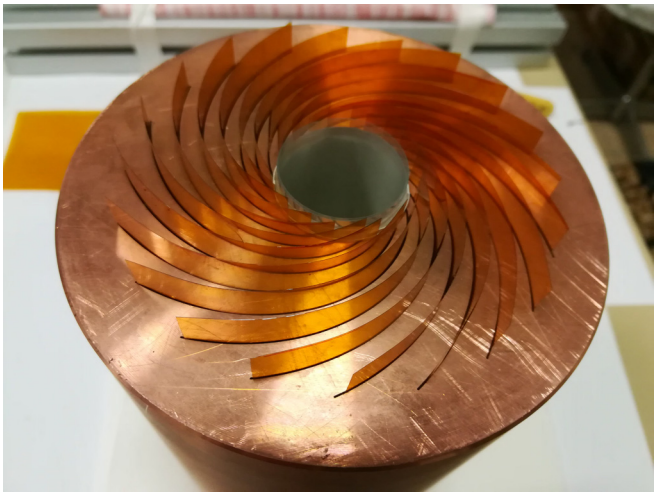

FIG. 2. Copper cylinder corresponding to the rotor of the Fury experiment [12]. The copper has been split over its entire height into narrow spirals into which kapton sheets have been inserted. The solid peripheral part (not split) was then eroded down to the kapton sheets. The spirals make an angle of 62° with the radial direction, corresponding to $\alpha = 28^\circ \approx 0.16\pi$.

governed by the need to obtain a high ratio of electrical conductivity for the first pair of materials, and magnetic permeability for the last two. Note that in the latter two cases, replacing tin$^{(\parallel)}$ with kapton$^{(\parallel)}$ would lead to a high ratio of electrical conductivity and magnetic permeability, which would be counterproductive to the dynamo, as shown in [16]. Indeed, from (39), in the double limit $\sigma_{\rm in} \gg 1$ and $\mu_{\rm in} \gg 1$, we have $k_{\sigma_{\rm in}} \sim k/s$ and $k_{\mu_{\rm in}} \sim k/s$, leading to $\Omega^c \gg 1$.

For the external medium we consider two materials in the liquid state, galinstan (Ga) and sodium (Na). The values of the electrical conductivity and magnetic permeability are taken at room temperature for galinstan and 100 °C for liquid sodium. In the latter case, the influence of temperature on the electrical conductivity must be taken into account, not only for sodium, but also for the materials constituting the rotor which will be also at 100 °C. The values of the electrical conductivities and magnetic permeabilities are collected in Table I, together with the corresponding values of $\sigma_{\rm in}$, $\mu_{\rm in}$, φ_σ, and φ_μ.

A. For $\alpha/\pi = 0.16$ rad

In Fig. 3(a) the critical magnetic Reynolds number $|\Omega^c|$ is plotted versus the dimensionless wave number k for the three rotors and the two external media, and $\alpha/\pi = 0.16$ rad. We find that $\Omega^c < 0$ for the copper$^{(\perp)}$/kapton$^{(\parallel)}$ rotor and $\Omega^c > 0$ for the other two, iron$^{(\perp)}$/tin$^{(\parallel)}$ and μ-metal$^{(\perp)}$/tin$^{(\parallel)}$, which means that with anisotropy as described in Fig. 1, the first rotor must rotate clockwise while the other two must rotate counterclockwise. Such a difference is common between electrical conductivity and magnetic permeability anisotropy [16]. The curves agree with the asymptotic limits derived in Appendix H: $\Omega^c \propto k^{-2}$ for $k \to 0$, and $\Omega^c \propto k$ for $k \to \infty$.

With an experimental realization in mind it is interesting to plot the results using dimensional quantities. In Fig. 3(b), the critical rotor's frequency f necessary to obtain the dynamo is plotted versus the magnetic vertical wavelength h for a rotor's radius $R = 5$ cm. They are defined as

$$f = \frac{|\Omega^c|}{2\pi \mu_{\rm in}^{\perp} \sigma_{\rm in}^{\perp} R^2}, \tag{40a}$$

$$h = 2\pi R/k. \tag{40b}$$

The minimum value of f with respect to h, and the corresponding value of h, are given in Table II.

TABLE I. The electrical conductivities $\sigma_{\rm in}^{\perp}$, $\sigma_{\rm in}^{\parallel}$, $\sigma_{\rm out}^{\perp}$, and $\sigma_{\rm out}^{\parallel}$ are given in units of $10^6\ \Omega^{-1}\,{\rm m}^{-1}$. The magnetic permeabilities $\mu_{\rm in}^{\perp}$, $\mu_{\rm in}^{\parallel}$, $\mu_{\rm out}^{\perp}$, and $\mu_{\rm out}^{\parallel}$ are given in units of $4\pi\times10^{-7}\ {\rm H\,m}^{-1}$. The parameters $\sigma_{\rm in}$, $\mu_{\rm in}$, φ_σ, and φ_μ are dimensionless. The numerical values of the electrical conductivity and magnetic permeability of the materials are taken from appropriate references given in Appendix I.

	Rotor						External medium				
								$\sigma_{\rm out}^{\perp}$	$\mu_{\rm out}^{\perp}$		
T (°C)	$\sigma_{\rm in}^{\perp}$	$\mu_{\rm in}^{\perp}$	$\sigma_{\rm in}^{\parallel}$	$\mu_{\rm in}^{\parallel}$	$\sigma_{\rm in}$	$\mu_{\rm in}$	Material	$\sigma_{\rm out}^{\parallel}$	$\mu_{\rm out}^{\parallel}$	φ_σ	φ_μ
	Cu$^{(\perp)}$		Ka$^{(\parallel)}$								
20	63	1	5×10^{-22}	1	13×10^{22}	0	Ga	3.86	1	0.06	1
100	47	1	2.5×10^{-19}	1	19×10^{19}	0	Na	10.6	1	0.23	1
	Fe$^{(\perp)}$		Sn$^{(\parallel)}$								
20	10.2	5×10^{3}	9.9	1	0.03	5×10^{3}	Ga	3.86	1	0.38	2×10^{-4}
100	6.9	5×10^{3}	7.2	1	−0.04	5×10^{3}	Na	10.6	1	1.53	2×10^{-4}
	μm$^{(\perp)}$		Sn$^{(\parallel)}$								
20	2.1	1.5×10^{5}	9.9	1	−0.79	1.5×10^{5}	Ga	3.86	1	1.85	6.7×10^{-6}
100	1.35	1.5×10^{5}	7.2	1	−0.81	1.5×10^{5}	Na	10.6	1	7.86	6.7×10^{-6}

For a copper$^{(\perp)}$/kapton$^{(\parallel)}$ rotor, the minimum critical frequency is $f_{\rm min}=91$ Hz in galinstan and $f_{\rm min}=48$ Hz in sodium, with a wavelength equal to $h=29$ and 25 cm respectively. From (40a), we note that increasing the rotor's radius R by a factor N would lead to a frequency N^2 times smaller and then to again more accessible dynamo action, provided that, after (40b), the rotor's height is N times larger. Then a minimum dynamo threshold frequency $f_{\rm min}=10$ Hz can be achieved with a rotor's radius $R=15$ cm and height $h=87$ cm in galinstan, and $R=11$ cm and $h=55$ cm in sodium. These values are also reported in Table II.

For an iron$^{(\perp)}$/tin$^{(\parallel)}$ rotor, the minimum critical frequency is $f_{\rm min}=36$ Hz in both galinstan and sodium, provided the rotor's height is equal to $h=50$ and 30 cm respectively (Table II). As in the previous case, using the property that the critical frequency decreases as R^{-2}, a minimum dynamo

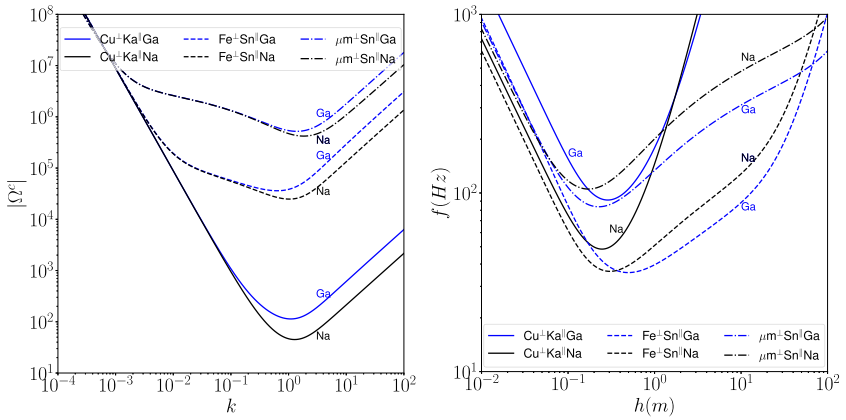

FIG. 3. The marginal curves of the dynamo instability for the three rotors copper$^{(\perp)}$/kapton$^{(\parallel)}$, iron$^{(\perp)}$/tin$^{(\parallel)}$, and μ-metal$^{(\perp)}$/tin$^{(\parallel)}$ and the two external liquid metals galinstan and sodium, and $\alpha=0.16\pi$. Left: The critical magnetic Reynolds number $|\Omega^c|$ is plotted vs the dimensionless magnetic wave number k. Right: The same marginal curves are plotted but using the two dimensional quantities: critical frequency f of the rotor and vertical magnetic wavelength h, for a rotor's radius $R=5$ cm.

TABLE II. The angle α, the rotor's radius R, the minimum dynamo frequency $f_{\min}$ with respect to h (Sec. V A) or with respect to both h and α for the values denoted with stars (Sec. V B), and the corresponding magnetic wavelength h are given for the three rotors and the two liquid external metals. The underlined values are inputs.

	Ga				Na (100 °C)			
	α/π (rad)	R (m)	$f_{\min}$ (Hz)	h (m)	α/π (rad)	R (m)	$f_{\min}$ (Hz)	h (m)
$Cu^{(\perp)}Ka^{(\parallel)}$	0.16	0.05	91	0.29	0.16	0.05	48	0.25
		0.15	10	0.87		0.11	10	0.55
	0.04*	0.05	53.5*	0.55*	0.07*	0.05	39.2*	0.36*
		0.12*	10	1.27*		0.1*	10	0.71*
$Fe^{(\perp)}Sn^{(\parallel)}$	0.16	0.05	36	0.5	0.16	0.05	36	0.3
		0.095	10	0.95		0.095	10	0.57
	0.006*	0.05	4.6*	4.9*	0.006*	0.05	6.75*	4.85*
		0.034*	10	3.32*		0.041*	10	4*
$\mu m^{(\perp)}Sn^{(\parallel)}$	0.16	0.05	84	0.23	0.16	0.05	105	0.17
		0.15	10	0.67		0.16	10	0.55
	0.001*	0.05	6.09*	36.6*	0.001*	0.05	9.47*	36.3*
		0.039*	10	28.6*		0.049*	10	35.3*

threshold frequency $f_{\min} = 10$ Hz can be achieved with a rotor's radius $R = 9.5$ cm and height $h = 95$ cm in galinstan, and $R = 9.5$ cm and $h = 57$ cm in sodium (Table II).

Similar conclusions can be reached for a μ-metal$^{(\perp)}$/tin$^{(\parallel)}$ rotor. The minimum critical frequency is $f_{\min} = 84$ Hz in galinstan and $f_{\min} = 105$ Hz in sodium, provided the rotor's height is $h = 23$ cm and $h = 17$ cm respectively (Table II). A minimum dynamo threshold frequency $f = 10$ Hz can be achieved with a rotor's radius $R = 15$ cm and height $h = 67$ cm in galinstan, and $R = 16$ cm and $h = 55$ cm in sodium (Table II).

In Fig. 4 the geometry of the horizontal magnetic induction field lines and current density lines is plotted in the (x, y) plane, for the three types of rotor (a) copper$^{(\perp)}$/kapton$^{(\parallel)}$, (b) iron$^{(\perp)}$/tin$^{(\parallel)}$, and (c) μ-metal$^{(\perp)}$/tin$^{(\parallel)}$ immersed in liquid sodium. The components B_r, B_θ, J_r, and J_θ are taken from (30), (31), (E11), (E14), (E12), and (E15), at the threshold $\gamma = 0$, with $\sigma_{\text{out}} = \mu_{\text{out}} = 0$, $k_{\sigma_{\text{out}}} = k_{\mu_{\text{out}}} = k$, $k_{\sigma_{\text{in}}}$, and $k_{\mu_{\text{in}}}$ taken from (25); σ_{in}, μ_{in}, φ_σ, and φ_μ from Table I; $\lambda_{\sigma_{\text{in}}}$, $\lambda_{\mu_{\text{in}}}$, $\lambda_{\sigma_{\text{out}}}$, and $\lambda_{\mu_{\text{out}}}$ from (G5)–(G8); and k satisfying (40 b) with h given in Table I.

The first observation is that the shape of the magnetic induction field lines is spiral, but in the opposite direction between case (a) and the other two cases (b) and (c). In case (a) it will be shown that the current density follows approximately the direction of the highest electrical conductivity,

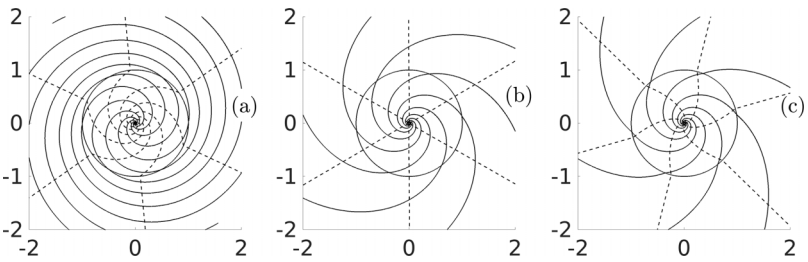

FIG. 4. Plot of the magnetic induction field lines (full) and the electric current lines (dashed) in the horizontal plane (x, y), at the dynamo threshold for a rotor immersed in liquid sodium, and made of (a) copper$^{(\perp)}$/kapton$^{(\parallel)}$, (b) iron$^{(\perp)}$/tin$^{(\parallel)}$, and (c) μ-metal$^{(\perp)}$/tin$^{(\parallel)}$.

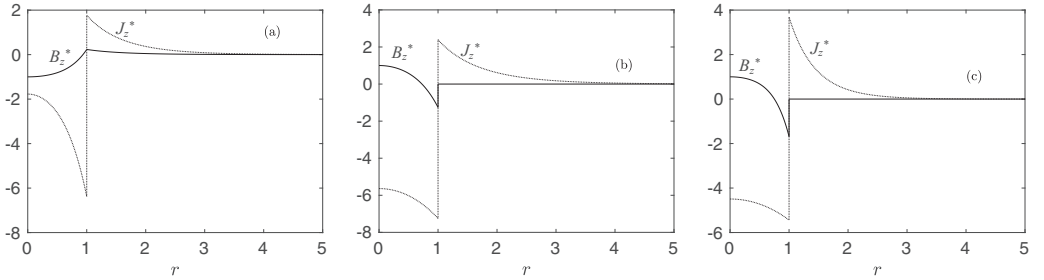

FIG. 5. Plot of $B_z^*(r) = -iB_z(r)/|B_z(0)|$ (full) and $J_z^*(r) = J_z(r)/|B_z(0)|$ (dashed), at the dynamo threshold for a rotor immersed in liquid sodium, and made of (a) copper$^{(\perp)}$/kapton$^{(\parallel)}$, (b) iron$^{(\perp)}$/tin$^{(\parallel)}$, and (c) μ-metal$^{(\perp)}$/tin$^{(\parallel)}$.

which is perpendicular to $\boldsymbol{q}$. Another observation is that the current density is always radial outside the rotor and, in case (b), inside the rotor too.

At the dynamo threshold $\gamma = 0$, and for an isotropic external medium implying $\sigma_{\text{out}} = 0$, from (E11) and (E12) we have

$$r < 1, \quad \frac{cs^2\sigma_{\text{in}}}{1 + s^2\sigma_{\text{in}}} J_r + sJ_\theta = 0 \tag{41a}$$

$$r > 1, \quad J_\theta = 0. \tag{41b}$$

From (41b), the current density lines are therefore radial straight lines for $r > 1$, as shown in Figs. 4(a), 4(b), and 4(c). In case (a) corresponding to a rotor made of copper$^{(\perp)}$ and kapton$^{(\parallel)}$, for $\alpha = 0.16\pi$ and $\sigma_{\text{in}} = 19 \times 10^{19}$, we have $s^2\sigma_{\text{in}} \gg 1$ implying from (41 a) that $cJ_r + sJ_\theta \approx 0$, or equivalently $\boldsymbol{J} \cdot \boldsymbol{q} \approx 0$ corresponding to current density lines perpendicular to $\boldsymbol{q}$, as shown in Fig. 4(a) for $r < 1$. In case (b), for $\alpha = 0.16\pi$ and $\sigma_{\text{in}} = -0.04$, we have $|\sigma_{\text{in}}s^2| \ll 1$ and $|\sigma_{\text{in}}sc| \ll 1$, implying from (41a) that $|J_\theta| \ll |J_r|$, and the current density lines are then approximately radial, as shown in Fig. 4(b) for $r < 1$.

In Fig. 5 the vertical components of the magnetic induction field and the current density are plotted versus r. The solution is normalized by the value of $|B_z|$ at $r = 0$. In cases (b) and (c) both B_z and J_z are discontinuous at $r = 1$, and B_z is much stronger in the rotor than in the external medium.

B. Varying values of α

In Fig. 6 the critical frequency f of the rotor (left scale) is plotted versus the vertical magnetic wavelength h (bottom scale), with the corresponding values of $|\Omega^c|$ (right scale) and k (top scale), for $R = 5 \times 10^{-2}$ m and different values of α. The dashed curve corresponds to $\alpha/\pi = 0.16$ rad, and the full curve corresponds to the one giving the minimum dynamo threshold with respect to both h and α. Such minimum frequency f_{min}, together with the corresponding values of α and h, is noted with stars in Table II. We see that the decrease of f_{min} is always accompanied by an increase of the magnetic wavelength h. For the copper$^{(\perp)}$/kapton$^{(\parallel)}$ rotor, f_{min} decreases from $f_{\text{min}} = 91$ Hz ($\alpha = 0.16\pi$) to $f_{\text{min}} = 53.5$ Hz ($\alpha = 0.04\pi$ rad) in galinstan and from $f_{\text{min}} = 48$ Hz ($\alpha = 0.16\pi$ rad) to $f_{\text{min}} = 39.2$ Hz ($\alpha = 0.07\pi$ rad) in sodium, while h increases from $h = 0.29$ to 0.55 m in galinstan and from $h = 0.25$ to 0.36 m in sodium. The increase of h is much more significant for the two rotors based on anisotropic magnetic permeability. For the iron$^{(\perp)}$/tin$^{(\parallel)}$ rotor, h increases from $h = 0.5$ m ($\alpha = 0.16\pi$) to $h = 4.9$ m ($\alpha = 0.006\pi$) in galinstan and from $h = 0.3$ m ($\alpha = 0.16\pi$) to $h = 4.85$ m ($\alpha = 0.006\pi$) in sodium. For the μ-metal$^{(\perp)}$/tin$^{(\parallel)}$ rotor, h increases from $h = 0.23$ m ($\alpha = 0.16\pi$) to $h = 36.6$ m ($\alpha = 0.001\pi$) in galinstan and from $h = 0.17$ m ($\alpha = 0.16\pi$) to $h = 36.3$ m ($\alpha = 0.001\pi$) in sodium. Such high values of h are not reasonable for experimental purposes.

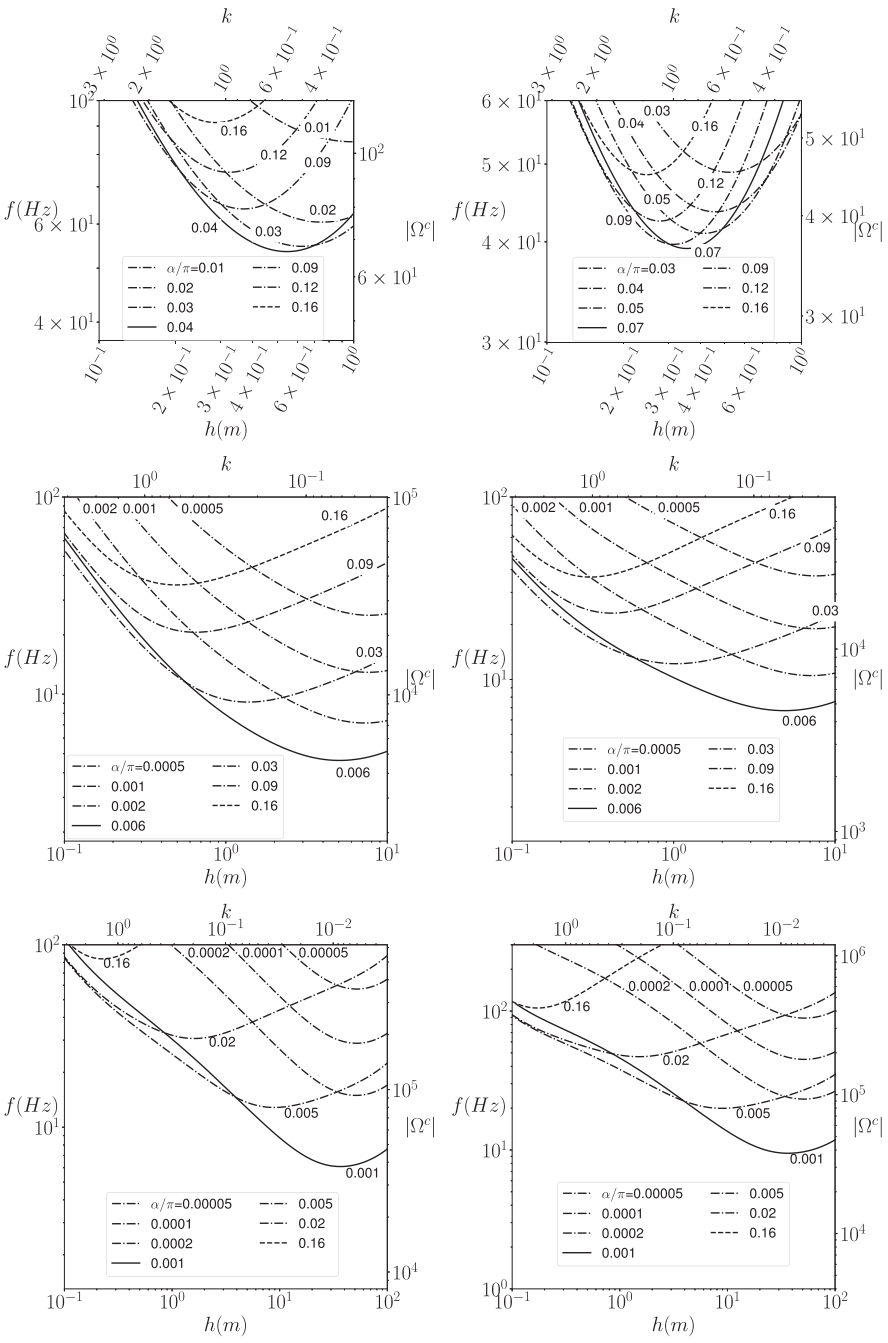

FIG. 6. The marginal curves of the dynamo instability, for $R = 5 \times 10^{-2}$ m and different values of α. Each top, middle, or bottom row corresponds to a rotor made of respectively copper$^{(\perp)}$/kapton$^{(\parallel)}$, iron$^{(\perp)}$/tin$^{(\parallel)}$, and μ-metal$^{(\perp)}$/tin$^{(\parallel)}$. Each left or right column corresponds to an external liquid metal made of respectively galinstan and sodium. Each curve corresponds to the critical frequency f of the rotor (left scale) plotted vs the vertical magnetic wavelength h (bottom scale). The corresponding values of $|\Omega^c|$ and k are given in the right and top scales. The dashed curves correspond to $\alpha/\pi = 0.16$ rad, and the full curve corresponds to the one giving the minimum dynamo threshold with respect to both h and α.

Now setting $f = 10$ Hz, from Table II we see that for a copper$^{(\perp)}$kapton$^{(\parallel)}$ rotor, the radius R does not change much, from $R = 0.15$ m ($\alpha = 0.16\pi$) to $R = 0.12$ m ($\alpha = 0.04\pi$) in galinstan and from $R = 0.11$ m ($\alpha = 0.16\pi$) to $R = 0.1$ m ($\alpha = 0.07\pi$) in sodium, and the magnetic wavelength h increases, from $h = 0.87$ m ($\alpha = 0.16\pi$) to $h = 1.27$ m ($\alpha = 0.04\pi$) in galinstan and from $h = 0.55$ m ($\alpha = 0.16\pi$) to $h = 0.71$ m ($\alpha = 0.07\pi$) in sodium. If we consider that the smaller the better, there is not much point in taking a value of α other than 0.16π rad.

VI. CONCLUSION

We have theoretically demonstrated how dynamo action can be produced by the rotation of an anisotropic rotor immersed in a liquid metal. The dynamo threshold depends on the size of the rotor, the materials used in its construction, and the external liquid metal. Considering three types of rotors, copper$^{(\perp)}$/kapton$^{(\parallel)}$, iron$^{(\perp)}$/tin$^{(\parallel)}$, and μ-metal$^{(\perp)}$/tin$^{(\parallel)}$ with an anisotropy given by $\alpha/\pi = 0.16$ rad, and two external liquid metals, galinstan and sodium, a minimum critical rotation frequency of 10 Hz is obtained for a rotor with a radius of 10 to 16 cm and a height of 55 to 95 cm, which are reasonable dimensions for experimental application.

A solution for the construction of the copper$^{(\perp)}$/kapton$^{(\parallel)}$ rotor is to use alternating layers of copper and kapton in logarithmic spirals as shown in Fig. 2, in order to mimic an anisotropic electrical conductivity. The two other rotors, iron$^{(\perp)}$/tin$^{(\parallel)}$ and μ-metal$^{(\perp)}$/tin$^{(\parallel)}$, can be designed in the same way, using iron or μ-metal instead of copper, and tin instead of kapton, in order to mimic this time an anisotropic magnetic permeability. The advantage of the first solution is that it has been experimentally proven [12]. For the latter two, attention should be paid to have a good electrical contact between tin and either iron or μ-metal; otherwise, in addition to the anisotropic magnetic permeability there will be an anisotropic electrical conductivity, the conjugation of both anisotropies leading to a much higher dynamo threshold [16]. A cylindrical piece of iron or μ-metal could be slit into narrow spirals, the slits then being filled with molten tin. In such arrangements of two materials with different electromagnetic properties, the quantities $\sigma_{\text{in}}^{\perp}$, $\sigma_{\text{in}}^{\parallel}$, $\mu_{\text{in}}^{\perp}$, and $\mu_{\text{in}}^{\parallel}$ will also depend on the relative thickness of each material (see Appendix J).

In the case of a copper$^{(\perp)}$/kapton$^{(\parallel)}$ rotor immersed in liquid sodium, the dynamo can be achieved with a cylindrical rotor of radius 11 cm and height 55 cm, rotating at a frequency of 10 Hz. Such a possibility may be of interest in a laboratory dynamo experiment like the one built in Maryland [21]. This experiment is composed of a rapidly rotating inner sphere immersed in a 3-m-diameter spherical shell filled with liquid sodium. Having an inner sphere made of an anisotropic material could certainly help to achieve the dynamo.

Instead of having a body immersed in liquid metal, one could, conversely, coat the inside of a vessel containing the liquid metal with an anisotropic material of a certain thickness. In this case, the outer part, the coating, would be anisotropic and the inner part, the liquid metal, would be isotropic. A sudden rotation of the container while the liquid metal is still at rest should be sufficient to start the dynamo. Such a solution without an internal rotor has the advantage of not requiring the passage of a shaft through the vessel and therefore not presenting a risk of leakage. This is, for example, a clear advantage of the Dresden experiment [22] in which a dynamo effect is predicted from a precessional motion of the liquid sodium contained in a (2×2)-m cylindrical shell. In this experiment, the addition of an anisotropic coating could promote the triggering of the dynamo.

APPENDIX A: DERIVATION OF (13)

The induction equation (9) is derived from (8d) and (8e), such that

$$\partial_t \boldsymbol{B} = \nabla \times (\boldsymbol{U} \times \boldsymbol{B}) - \nabla \times [\sigma_{ij}]^{-1} \boldsymbol{J}, \tag{A1}$$

with, from (8a) and (8c),

$$\boldsymbol{J} = \nabla \times [\mu_{ij}]^{-1} \boldsymbol{B}. \tag{A2}$$

Assuming axisymmetry ($\partial_\theta = 0$) and considering the solenoidality of $\boldsymbol{B}$ given by (8b), the curl of the cross product of $\boldsymbol{U} = r\tilde{\Omega}(r)\boldsymbol{E}_\theta$ by $\boldsymbol{B} = (B_r, B_\theta, B_z)\exp(\gamma t + ikz)$ takes the form

$$\nabla \times (\boldsymbol{U} \times \boldsymbol{B}) = r\tilde{\Omega}' B_r \boldsymbol{e}_\theta, \tag{A3}$$

where, from now on, the exponential term is dropped for convenience. From the definition (10a) of $[\sigma_{ij}]^{-1}$, we have

$$[\sigma_{ij}]^{-1}\boldsymbol{J} = (\tilde{\varphi}_\sigma \sigma_{\text{in}}^{\perp})^{-1} \begin{pmatrix} (1+\tilde{\sigma}c^2)J_r + \tilde{\sigma}csJ_\theta \\ \tilde{\sigma}csJ_r + (1+\tilde{\sigma}s^2)J_\theta \\ J_z \end{pmatrix}. \tag{A4}$$

Taking the curl leads to

$$\nabla \times [\sigma_{ij}]^{-1}\boldsymbol{J} = (\tilde{\varphi}_\sigma \sigma_{\text{in}}^{\perp})^{-1} \begin{pmatrix} -ik[\tilde{\sigma}csJ_r + (1+\tilde{\sigma}s^2)J_\theta] \\ ik^{-1}[D_k(J_r) + \tilde{\sigma}c^2k^2J_r + \tilde{\sigma}csk^2J_\theta] \\ \frac{1}{r}\partial_r(r[\tilde{\sigma}csJ_r + (1+\tilde{\sigma}s^2)J_\theta]) \end{pmatrix}, \tag{A5}$$

where, again, $D_\nu(X) = \nu^2 X - \partial_r[\frac{1}{r}\partial_r(rX)]$, and with $J_z = ik^{-1}\frac{1}{r}\partial_r(rJ_r)$ coming from the solenoidality of the current density.

Similarly, we find that

$$\boldsymbol{J} = \nabla \times [\mu_{ij}]^{-1}\boldsymbol{B} = (\tilde{\varphi}_\mu \mu_{\text{in}}^{\perp})^{-1} \begin{pmatrix} -ik[\tilde{\mu}csB_r + (1+\tilde{\mu}s^2)B_\theta] \\ ik^{-1}[D_k(B_r) + \tilde{\mu}c^2k^2B_r + \tilde{\mu}csk^2B_\theta] \\ \frac{1}{r}\partial_r(r[\tilde{\mu}csB_r + (1+\mu s^2)B_\theta]) \end{pmatrix}. \tag{A6}$$

Combining (A5) and (A6) leads to

$$\nabla \times [\sigma_{ij}]^{-1}[\nabla \times [\mu_{ij}]^{-1}\boldsymbol{B}] = (\tilde{\varphi}_\sigma \tilde{\varphi}_\mu \sigma_{\text{in}}^{\perp}\mu_{\text{in}}^{\perp})^{-1} \begin{pmatrix} \tilde{F} \\ \tilde{G} \\ ik^{-1}\left(\frac{1}{r}\partial_r(r\tilde{F})\right) \end{pmatrix}, \tag{A7}$$

with

$$\tilde{F} = \tilde{\mu}c^2k^2B_r + (1+\tilde{\sigma}s^2)D_k(B_r) - k^2cs(\tilde{\sigma} - \tilde{\mu})B_\theta, \tag{A8}$$

$$\tilde{G} = -cs(\tilde{\sigma} - \tilde{\mu})D_k(B_r) + \tilde{\sigma}k^2c^2B_\theta + (1+\tilde{\mu}s^2)D_k(B_\theta). \tag{A9}$$

Combining (A1), (A2), (A3), and (A7) leads to (13).

APPENDIX B: DERIVATION OF (28)

Rewriting (13) in the dimensionless form

$$D_k(B_r) = -[\tilde{\gamma}B_r + \tilde{\mu}c^2k^2B_r + \tilde{\sigma}s^2D_k(B_r) - cs(\tilde{\sigma} - \tilde{\mu})k^2B_\theta], \tag{B1a}$$

$$D_k(B_\theta) = -[\tilde{\gamma}B_\theta + \tilde{\sigma}c^2k^2B_\theta + \tilde{\mu}s^2D_k(B_\theta) - cs(\tilde{\sigma} - \tilde{\mu})D_k(B_r)], \tag{B1b}$$

and considering the linear combination c [(B1a)] + s [(B1b)], leads to

$$(1+\tilde{\mu}s^2)D_k(cB_r + sB_\theta) = -(\tilde{\gamma} + \tilde{\mu}c^2k^2)(cB_r + sB_\theta). \tag{B2}$$

Then, using the identity

$$(1+\tilde{\mu}s^2)D_k(X) = (1+\tilde{\mu}s^2)D_{k_{\tilde{\mu}}}(X) - (\tilde{\gamma} + \tilde{\mu}c^2k^2)X, \tag{B3}$$

we find that

$$D_{k_{\tilde{\mu}}}(cB_r + sB_\theta) = 0. \tag{B4}$$

In a similar way, considering the linear combination sD_k [(B1a)] + ck^2 [(B1b)] leads to

$$(1+\tilde{\sigma}s^2)D_k[sD_k(B_r)-ck^2B_\theta] = -(\tilde{\gamma}+\tilde{\sigma}c^2k^2)[sD_k(B_r)-ck^2B_\theta]. \tag{B5}$$

Then, using the identity

$$(1+\tilde{\sigma}s^2)D_k(X) = (1+\tilde{\sigma}s^2)D_{k_{\tilde{\sigma}}}(X) - (\tilde{\gamma}+\tilde{\sigma}c^2k^2)X, \tag{B6}$$

we find that

$$D_{k_{\tilde{\sigma}}}[sD_k(B_r)-ck^2B_\theta] = 0. \tag{B7}$$

APPENDIX C: DERIVATION OF (31)

To obtain B_θ from B_r by replacing (30) in (27a), we need to calculate $D_{k_{\tilde{\sigma}}}(B_r)$, given by

$$D_{k_{\tilde{\sigma}}}(B_r) = \begin{cases} r<1, & -s\lambda_{\mu_{\text{in}}}\frac{D_{k_{\sigma_{\text{in}}}}[I_1(k_{\mu_{\text{in}}}r)]}{I_1(k_{\mu_{\text{in}}})} \\ r>1, & -s\lambda_{\mu_{\text{out}}}\frac{D_{k_{\sigma_{\text{out}}}}[K_1(k_{\mu_{\text{out}}}r)]}{K_1(k_{\mu_{\text{out}}})} \end{cases}. \tag{C1}$$

With the help of the identity (26) we have

$$D_{k_{\tilde{\sigma}}}(B_r) = \begin{cases} r<1, & -s\lambda_{\mu_{\text{in}}}\left(k_{\sigma_{\text{in}}}^2-k_{\mu_{\text{in}}}^2\right)\frac{I_1(k_{\mu_{\text{in}}}r)}{I_1(k_{\mu_{\text{in}}})} \\ r>1, & -s\lambda_{\mu_{\text{out}}}\left(k_{\sigma_{\text{out}}}^2-k_{\mu_{\text{out}}}^2\right)\frac{K_1(k_{\mu_{\text{out}}}r)}{K_1(k_{\mu_{\text{out}}})} \end{cases}. \tag{C2}$$

Then replacing $k_{\sigma_{\text{in}}}$, $k_{\mu_{\text{in}}}$, $k_{\sigma_{\text{out}}}$, and $k_{\mu_{\text{out}}}$ by their expressions given in (25) and performing some additional algebra leads to (31).

APPENDIX D: DERIVATION OF THE BOUNDARY CONDITION (34)

To derive the boundary condition (34) we need to calculate the expression of $\partial_r B_r$ at any r. From the following identities satisfied for any ν,

$$\partial_r[I_1(\nu r)] = \nu I_0(\nu r) - \frac{1}{r}I_1(\nu r), \tag{D1}$$

$$\partial_r[K_1(\nu r)] = -\nu K_0(\nu r) - \frac{1}{r}K_1(\nu r), \tag{D2}$$

the expression of $\partial_r B_r$ is obtained by deriving (30):

$$\partial_r B_r = \begin{cases} r\leqslant 1, & -s\frac{\lambda_{\sigma_{\text{in}}}}{I_1(k_{\sigma_{\text{in}}})}\left[k_{\sigma_{\text{in}}}I_0(k_{\sigma_{\text{in}}}r)-\frac{1}{r}I_1(k_{\sigma_{\text{in}}}r)\right] - s\frac{\lambda_{\mu_{\text{in}}}}{I_1(k_{\mu_{\text{in}}})}\left[k_{\mu_{\text{in}}}I_0(k_{\mu_{\text{in}}}r)-\frac{1}{r}I_1(k_{\mu_{\text{in}}}r)\right] \\ r\geqslant 1, & s\frac{\lambda_{\sigma_{\text{out}}}}{K_1(k_{\sigma_{\text{out}}})}\left[k_{\sigma_{\text{out}}}K_0(k_{\sigma_{\text{out}}}r)+\frac{1}{r}K_1(k_{\sigma_{\text{out}}}r)\right] s\frac{\lambda_{\mu_{\text{out}}}}{K_1(k_{\mu_{\text{out}}})}\left[k_{\mu_{\text{out}}}K_0(k_{\mu_{\text{out}}}r)+\frac{1}{r}K_1(k_{\mu_{\text{out}}}r)\right] \end{cases}. \tag{D3}$$

Then, using (D3) in (22) leads to (34).

APPENDIX E: DERIVATION OF THE CURRENT DENSITY $\boldsymbol{J}$

The current density $\boldsymbol{J}$ given in (A6) can be written, in its renormalized form, as

$$\boldsymbol{J} = \tilde{\varphi}_\mu^{-1}\begin{pmatrix} -ik\phi \\ ik^{-1}[D_k(B_r)+\tilde{\mu}c^2k^2B_r+\tilde{\mu}csk^2B_\theta] \\ \frac{1}{r}\partial_r(r\phi) \end{pmatrix} \tag{E1}$$

with $\phi = \tilde{\mu}csB_r + (1+\tilde{\mu}s^2)B_\theta$.

Replacing B_r and B_θ by their expressions (30) and (31) leads to

$$\phi = \begin{cases} r < 1, & c\left[\lambda_{\sigma_{\text{in}}} \frac{I_1(k_{\sigma_{\text{in}}} r)}{I_1(k_{\sigma_{\text{in}}})} + \frac{s^2\gamma}{c^2k^2}\lambda_{\mu_{\text{in}}} \frac{I_1(k_{\mu_{\text{in}}} r)}{I_1(k_{\mu_{\text{in}}})}\right] \\ r > 1, & c\left[\lambda_{\sigma_{\text{out}}} \frac{K_1(k_{\sigma_{\text{out}}} r)}{K_1(k_{\sigma_{\text{out}}})} + \varphi_\sigma\varphi_\mu \frac{s^2\gamma}{c^2k^2}\lambda_{\mu_{\text{out}}} \frac{K_1(k_{\mu_{\text{out}}} r)}{K_1(k_{\mu_{\text{out}}})}\right] \end{cases}, \tag{E2}$$

and therefore to J_r.

Using the relations (D1) and (D2) written in the form

$$\frac{1}{r}\partial_r[rI_1(\nu r)] = \nu I_0(\nu r), \tag{E3}$$

$$\frac{1}{r}\partial_r[rK_1(\nu r)] = -\nu K_0(\nu r) \tag{E4}$$

leads to

$$\frac{1}{r}\partial_r(r\phi) = \begin{cases} r < 1, & c\left[\lambda_{\sigma_{\text{in}}} k_{\sigma_{\text{in}}} \frac{I_0(k_{\sigma_{\text{in}}} r)}{I_1(k_{\sigma_{\text{in}}})} + \frac{s^2\gamma}{c^2k^2}\lambda_{\mu_{\text{in}}} k_{\mu_{\text{in}}} \frac{I_0(k_{\mu_{\text{in}}} r)}{I_1(k_{\mu_{\text{in}}})}\right] \\ r > 1, & -c\left[\lambda_{\sigma_{\text{out}}} k_{\sigma_{\text{out}}} \frac{K_0(k_{\sigma_{\text{out}}} r)}{K_1(k_{\sigma_{\text{out}}})} + \varphi_\sigma\varphi_\mu \frac{s^2\gamma}{c^2k^2}\lambda_{\mu_{\text{out}}} k_{\mu_{\text{out}}} \frac{K_0(k_{\mu_{\text{out}}} r)}{K_1(k_{\mu_{\text{out}}})}\right] \end{cases} \tag{E5}$$

and therefore to J_z.

Using (B3), we find that

$$D_k(B_r) + \tilde{\mu}c^2k^2B_r + \tilde{\mu}csk^2B_\theta = D_{k_{\tilde{\mu}}}(B_r) + \frac{\tilde{\mu}csk^2\phi - \tilde{\gamma}B_r}{1 + \tilde{\mu}s^2}. \tag{E6}$$

From the expression of B_r given by (30), we have

$$D_{k_{\tilde{\mu}}}(B_r) = \begin{cases} r < 1, & -\frac{s\lambda_{\sigma_{\text{in}}}}{I_1(k_{\sigma_{\text{in}}})} D_{k_{\mu_{\text{in}}}}\left[I_1\left(k_{\sigma_{\text{in}}} r\right)\right] \\ r > 1, & -\frac{s\lambda_{\sigma_{\text{out}}}}{K_1(k_{\sigma_{\text{out}}})} D_{k_{\mu_{\text{out}}}}\left[K_1\left(k_{\sigma_{\text{out}}} r\right)\right] \end{cases}. \tag{E7}$$

Using (26) leads to

$$D_{k_{\tilde{\mu}}}(B_r) = \begin{cases} r < 1, & -\frac{s\lambda_{\sigma_{\text{in}}}}{I_1(k_{\sigma_{\text{in}}})}\left(k_{\mu_{\text{in}}}^2 - k_{\sigma_{\text{in}}}^2\right) I_1\left(k_{\sigma_{\text{in}}} r\right) \\ r > 1, & -\frac{s\lambda_{\sigma_{\text{out}}}}{K_1(k_{\sigma_{\text{out}}})}\left(k_{\mu_{\text{out}}}^2 - k_{\sigma_{\text{out}}}^2\right) K_1\left(k_{\sigma_{\text{out}}} r\right) \end{cases}, \tag{E8}$$

where we used the identity $D_\nu[I_1(k_\nu r)] = D_\nu[K_1(k_\nu r)] = 0$. After some algebra we find that

$$D_{k_{\tilde{\mu}}}(B_r) + \frac{\tilde{\mu}csk^2\phi - \tilde{\gamma}B_r}{1 + \tilde{\mu}s^2} = \tag{E9}$$

$$\begin{cases} r < 1, & \lambda_{\sigma_{\text{in}}} sk^2\left(\frac{\sigma_{\text{in}}c^2 + \gamma/k^2}{1 + \sigma_{\text{in}}s^2}\right)\frac{I_1(k_{\sigma_{\text{in}}} r)}{I_1(k_{\sigma_{\text{in}}})} + s\gamma\lambda_{\mu_{\text{in}}}\frac{I_1(k_{\mu_{\text{in}}} r)}{I_1(k_{\mu_{\text{in}}})} \\ r > 1, & \lambda_{\sigma_{\text{out}}} sk^2\left(\frac{\sigma_{\text{out}}c^2 + \varphi_\sigma\varphi_\mu\gamma/k^2}{1 + \sigma_{\text{out}}s^2}\right)\frac{K_1(k_{\sigma_{\text{out}}} r)}{K_1(k_{\sigma_{\text{out}}})} + s\varphi_\sigma\varphi_\mu\gamma\lambda_{\mu_{\text{out}}}\frac{K_1(k_{\mu_{\text{out}}} r)}{K_1(k_{\mu_{\text{out}}})} \end{cases}, \tag{E10}$$

leading to J_θ.

Then the current density takes the following form for $r < 1$,

$$J_r = -ikc\left[\lambda_{\sigma_{\text{in}}}\frac{I_1\left(k_{\sigma_{\text{in}}} r\right)}{I_1\left(k_{\sigma_{\text{in}}}\right)} + \frac{s^2\gamma}{c^2k^2}\lambda_{\mu_{\text{in}}}\frac{I_1\left(k_{\mu_{\text{in}}} r\right)}{I_1\left(k_{\mu_{\text{in}}}\right)}\right], \tag{E11}$$

$$J_\theta = iks\left[\lambda_{\sigma_{\text{in}}}\left(\frac{\sigma_{\text{in}}c^2 + \gamma/k^2}{1 + \sigma_{\text{in}}s^2}\right)\frac{I_1\left(k_{\sigma_{\text{in}}} r\right)}{I_1\left(k_{\sigma_{\text{in}}}\right)} + \frac{\gamma}{k^2}\lambda_{\mu_{\text{in}}}\frac{I_1\left(k_{\mu_{\text{in}}} r\right)}{I_1\left(k_{\mu_{\text{in}}}\right)}\right], \tag{E12}$$

$$J_z = c\left[\lambda_{\sigma_{\text{in}}} k_{\sigma_{\text{in}}}\frac{I_0\left(k_{\sigma_{\text{in}}} r\right)}{I_1\left(k_{\sigma_{\text{in}}}\right)} + \frac{s^2\gamma}{c^2k^2}\lambda_{\mu_{\text{in}}} k_{\mu_{\text{in}}}\frac{I_0\left(k_{\mu_{\text{in}}} r\right)}{I_1\left(k_{\mu_{\text{in}}}\right)}\right], \tag{E13}$$

and the following form for $r > 1$:

$$J_r = -ikc\varphi_\mu^{-1}\left[\lambda_{\sigma_{\text{out}}}\frac{K_1\left(k_{\sigma_{\text{out}}}r\right)}{K_1\left(k_{\sigma_{\text{out}}}\right)} + \varphi_\sigma\varphi_\mu\frac{s^2\gamma}{c^2k^2}\lambda_{\mu_{\text{out}}}\frac{K_1\left(k_{\mu_{\text{out}}}r\right)}{K_1\left(k_{\mu_{\text{out}}}\right)}\right], \tag{E14}$$

$$J_\theta = iks\varphi_\mu^{-1}\left[\lambda_{\sigma_{\text{out}}}\left(\frac{\sigma_{\text{out}}c^2 + \varphi_\sigma\varphi_\mu\frac{\gamma}{k^2}}{1+\sigma_{\text{out}}s^2}\right)\frac{K_1\left(k_{\sigma_{\text{out}}}r\right)}{K_1\left(k_{\sigma_{\text{out}}}\right)} + \varphi_\sigma\varphi_\mu\frac{\gamma}{k^2}\lambda_{\mu_{\text{out}}}\frac{K_1\left(k_{\mu_{\text{out}}}r\right)}{K_1\left(k_{\mu_{\text{out}}}\right)}\right]. \tag{E15}$$

$$J_z = -c\varphi_\mu^{-1}\left[\lambda_{\sigma_{\text{out}}}k_{\sigma_{\text{out}}}\frac{K_0\left(k_{\sigma_{\text{out}}}r\right)}{K_1\left(k_{\sigma_{\text{out}}}\right)} + \varphi_\sigma\varphi_\mu\frac{s^2\gamma}{c^2k^2}\lambda_{\mu_{\text{out}}}k_{\mu_{\text{out}}}\frac{K_0\left(k_{\mu_{\text{out}}}r\right)}{K_1\left(k_{\mu_{\text{out}}}\right)}\right]. \tag{E16}$$

APPENDIX F: DERIVATION OF Bz

From (19) we have

$$B_z = ik^{-1}\left(\frac{B_r}{r} + \partial_r B_r\right). \tag{F1}$$

Then replacing (30) and (D3) in (F1) leads to

$$B_z = ik^{-1}s\begin{cases} r<1, & -\left[\lambda_{\sigma_{\text{in}}}k_{\sigma_{\text{in}}}\frac{I_0(k_{\sigma_{\text{in}}}r)}{I_1(k_{\sigma_{\text{in}}})} + \lambda_{\mu_{\text{in}}}k_{\mu_{\text{in}}}\frac{I_0(k_{\mu_{\text{in}}}r)}{I_1(k_{\mu_{\text{in}}})}\right] \\ r>1, & \lambda_{\sigma_{\text{out}}}k_{\sigma_{\text{out}}}\frac{K_0(k_{\sigma_{\text{out}}}r)}{K_1(k_{\sigma_{\text{out}}})} + \lambda_{\mu_{\text{out}}}k_{\mu_{\text{out}}}\frac{K_0(k_{\mu_{\text{out}}}r)}{K_1(k_{\mu_{\text{out}}})}\end{cases}. \tag{F2}$$

APPENDIX G: EIGENVECTORS FOR $\gamma = 0$ AND $k_{\sigma_{\text{out}}} = k_{\mu_{\text{out}}} = k$

For $\gamma = 0$ and $k_{\sigma_{\text{out}}} = k_{\mu_{\text{out}}} = k$, Eqs. (32), (33), (34), and (36) take the following expressions:

$$\lambda_{\sigma_{\text{in}}} + \lambda_{\mu_{\text{in}}} = \lambda_{\sigma_{\text{out}}} + \lambda_{\mu_{\text{out}}}, \tag{G1}$$

$$\lambda_{\sigma_{\text{in}}} = \varphi_\mu^{-1}\lambda_{\sigma_{\text{out}}}, \tag{G2}$$

$$\lambda_{\sigma_{\text{in}}}\Phi\left(k_{\sigma_{\text{in}}}\right) + \lambda_{\mu_{\text{in}}}\Phi\left(k_{\mu_{\text{in}}}\right) = -\varphi_\mu^{-1}\left(\lambda_{\sigma_{\text{out}}} + \lambda_{\mu_{\text{out}}}\right)\Psi(k), \tag{G3}$$

$$\frac{s}{c}\left(\lambda_{\sigma_{\text{in}}} + \lambda_{\mu_{\text{in}}}\right)\Omega^c = \lambda_{\sigma_{\text{in}}}\Phi\left(k_{\sigma_{\text{in}}}\right) + \varphi_\sigma^{-1}\lambda_{\sigma_{\text{out}}}\Psi(k), \tag{G4}$$

with $\Phi(x)$, $\Psi(x)$, $k_{\sigma_{\text{in}}}$, and $k_{\mu_{\text{in}}}$ defined in (37) and (25). In (G4), replacing Ω^c by its expression (39) leads to the following expressions for $\lambda_{\sigma_{\text{in}}}$, $\lambda_{\mu_{\text{in}}}$, $\lambda_{\sigma_{\text{out}}}$, and $\lambda_{\mu_{\text{out}}}$, given to within one multiplication factor:

$$\lambda_{\sigma_{\text{in}}} = -\Phi\left(k_{\mu_{\text{in}}}\right) - \varphi_\mu^{-1}\Psi(k), \tag{G5}$$

$$\lambda_{\mu_{\text{in}}} = \Phi\left(k_{\sigma_{\text{in}}}\right) + \varphi_\mu^{-1}\Psi(k), \tag{G6}$$

$$\lambda_{\sigma_{\text{out}}} = -\varphi_\mu\Phi\left(k_{\mu_{\text{in}}}\right) - \Psi(k), \tag{G7}$$

$$\lambda_{\mu_{\text{out}}} = \Phi\left(k_{\sigma_{\text{in}}}\right) + (\varphi_\mu - 1)\Phi\left(k_{\mu_{\text{in}}}\right) + \Psi(k). \tag{G8}$$

Then replacing $\lambda_{\sigma_{\text{in}}}$, $\lambda_{\mu_{\text{in}}}$, $\lambda_{\sigma_{\text{out}}}$, and $\lambda_{\mu_{\text{out}}}$ in (30), (31), (F2), and (E11)–(E16) leads to the eigenvectors $\boldsymbol{B}$ and $\boldsymbol{J}$ which are plotted in Fig. 4.

APPENDIX H: ASYMPTOTICS IN k OF Ω^c

In the limit $x \to 0$, after [23], we have

$$I_0(x) \propto 1 + x^2/4, \quad I_1(x) \propto x/2 + x^3/16, \quad K_0(x) \propto -\ln(x), \quad K_1(x) \propto x^{-1}, \tag{H1}$$

TABLE III. The temperature T is given in Kelvin, the electrical resistivity ρ is given in units of $10^{-8}\ \Omega\,\mathrm{m}$, and temperature coefficient of resistivity a is given in units of $10^{-3}\ \mathrm{K}^{-1}$. The electrical conductivity at temperature T (resp. 373 K) is denoted by $\sigma(T)$ [resp. $\sigma(373\ \mathrm{K})$] and is given in units of $10^{6}\ \Omega^{-1}\,\mathrm{m}^{-1}$. The maximal relative magnetic permeability μ_r is dimensionless.

	T(K)	ρ	a	$\sigma(T)$	$\sigma(373\ \mathrm{K})$	μ_r
Ga	303	25.9		3.86		1
Na	371	9.43		10.6		1
μm	293	48	6.8	2.08	1.35	1.5×10^5
Fe	300	9.8	6.5	10.2	6.9	5×10^5
Cu	293	1.58	4.3	63.29	47.1	1
Sn	293	10.1	4.6	9.9	7.24	1
Ka	293	2×10^{23}		5×10^{-22}		1
Ka	473	4×10^{20}		2.5×10^{-19}		1
Ni	293	6.2	6.8	16.1	10.4	1

leading to

$$\Phi(x) \propto 2(1 + x^2/8), \quad \Psi(x) \propto -x^2 \ln(x), \tag{H2}$$

and then, from (39), to the following asymptotic behavior for $k \to 0$:

$$\Omega^c \propto -\frac{16c}{s} k^{-2} \left(\frac{1+\sigma_{\mathrm{in}}}{1+\sigma_{\mathrm{in}} s^2} - \frac{1+\mu_{\mathrm{in}}}{1+\mu_{\mathrm{in}} s^2} \right)^{-1}. \tag{H3}$$

In the limit $x \to \infty$, after [23], we have

$$I_0(x) \propto I_1(x) \propto \frac{e^x}{\sqrt{2\pi x}}, \quad K_0(x) \propto K_1(x) \propto \sqrt{\frac{\pi}{2x}}\, e^{-x}, \tag{H4}$$

leading to

$$\Phi(x) \propto \Psi(x) \propto x, \tag{H5}$$

and then, from (39), to the following asymptotic behavior for $k \to \infty$:

$$\Omega^c \propto -\frac{c}{s} k \frac{\left(\varphi_\sigma^{-1} + \sqrt{\frac{1+\sigma_{\mathrm{in}}}{1+\sigma_{\mathrm{in}} s^2}}\right)\left(\varphi_\mu^{-1} + \sqrt{\frac{1+\mu_{\mathrm{in}}}{1+\mu_{\mathrm{in}} s^2}}\right)}{\sqrt{\frac{1+\sigma_{\mathrm{in}}}{1+\sigma_{\mathrm{in}} s^2}} - \sqrt{\frac{1+\mu_{\mathrm{in}}}{1+\mu_{\mathrm{in}} s^2}}}. \tag{H6}$$

APPENDIX I: REFERENCES TO ESTIMATE THE ELECTRICAL AND MAGNETIC PROPERTIES OF THE MATERIALS CONSIDERED IN TABLE I

In Table III, for each material the value of the electrical resistivity ρ at some temperature T is taken from [24], except for kapton, that is taken from [25] for the two temperatures 29 and 473 K. For Fe, Cu, Sn, and μm, assuming a linear behavior of the resistivity with temperature, and for a temperature coefficient resistivity taken from [24], the resistivity and then the conductivity at 373 K can be estimated. As μ-metal is made of about 80% nickel, we assume that it has the same temperature coefficient resistivity as nickel. The values of the relative magnetic permeability μ_r are taken from [26], except for μ-metal, that is taken from [27].

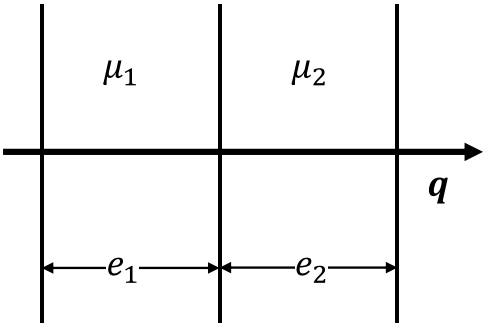

FIG. 7. Illustration of two layers, both perpendicular to $\boldsymbol{q}$, of thickness and permeability e_1, μ_1 and e_2, μ_2 respectively. The network is taken periodic in the $\boldsymbol{q}$ direction.

APPENDIX J: MEAN PARALLEL AND PERPENDICULAR MAGNETIC PERMEABILITY IN A PERIODIC NETWORK OF PARALLEL LAYERS OF DIFFERENT THICKNESS AND PERMEABILITY

Suppose a periodic network of parallel layers with alternated thickness e_1 and e_2 and alternated magnetic permeability μ_1 and μ_2, as illustrated in Fig. 7. All layers are perpendicular to a vector $\boldsymbol{q}$. Therefore the direction parallel to $\boldsymbol{q}$ is called parallel and the directions perpendicular to $\boldsymbol{q}$ are called perpendicular. In each of layers 1 and 2 that constitute a period of the network, we have

$$\boldsymbol{H}_1 = \boldsymbol{B}_1/\mu_1, \quad \boldsymbol{H}_2 = \boldsymbol{B}_2/\mu_2. \tag{J1}$$

Suppose now that a current field is applied in the direction of $\boldsymbol{q}$. Then, from (8c), a magnetic field $\boldsymbol{H}^\perp$ is generated in the direction perpendicular to $\boldsymbol{q}$ in all layers, $\boldsymbol{H}_1 = \boldsymbol{H}_2 = \boldsymbol{H}^\perp$, implying the following induction fields:

$$\boldsymbol{B}_1 = \mu_1 \boldsymbol{H}^\perp, \quad \boldsymbol{B}_2 = \mu_2 \boldsymbol{H}^\perp. \tag{J2}$$

Then a mean magnetic induction can be calculated as

$$\boldsymbol{B} = \frac{e_1 \boldsymbol{B}_1 + e_2 \boldsymbol{B}_2}{e_1 + e_2}. \tag{J3}$$

Replacing (J2) in (J3) and looking for $\mu^\perp$ such that $\boldsymbol{B} = \mu^\perp \boldsymbol{H}^\perp$, we find the following mean perpendicular magnetic permeability:

$$\mu^\perp = \frac{e_1\mu_1 + e_2\mu_2}{e_1 + e_2}. \tag{J4}$$

Applying now an induction field $\boldsymbol{B}^\parallel$ which is parallel to $\boldsymbol{q}$, then from (8b) we have $\boldsymbol{B}_1 = \boldsymbol{B}_2 = \boldsymbol{B}^\parallel$, implying the following magnetic fields in the direction parallel to $\boldsymbol{q}$:

$$\boldsymbol{H}_1 = \boldsymbol{B}^\parallel/\mu_1, \quad \boldsymbol{H}_2 = \boldsymbol{B}^\parallel/\mu_2. \tag{J5}$$

Then a mean magnetic field can be calculated as

$$\boldsymbol{H} = \frac{e_1 \boldsymbol{H}_1 + e_2 \boldsymbol{H}_2}{e_1 + e_2}. \tag{J6}$$

Replacing (J5) in (J6) and looking for $\mu^\parallel$ such that $\boldsymbol{H} = \boldsymbol{B}^\parallel/\mu^\parallel$, we find the following mean parallel magnetic permeability:

$$(\mu^\parallel)^{-1} = \frac{e_1\mu_1^{-1} + e_2\mu_2^{-1}}{e_1 + e_2}. \tag{J7}$$

TABLE IV. The electrical conductivities σ_1, σ_2, $\sigma_{\text{in}}^{\perp}$, $\sigma_{\text{in}}^{\parallel}$, $\sigma_{\text{out}}^{\perp}$, and $\sigma_{\text{out}}^{\parallel}$ are given in units of $10^6\ \Omega^{-1}\ \text{m}^{-1}$. The magnetic permeabilities μ_1, μ_2, $\mu_{\text{in}}^{\perp}$, $\mu_{\text{in}}^{\parallel}$, $\mu_{\text{out}}^{\perp}$, and $\mu_{\text{out}}^{\parallel}$ are given in units of $4\pi \times 10^{-7}\ \text{H m}^{-1}$. The parameters σ_{in}, μ_{in}, φ_σ, and φ_μ are dimensionless.

	Rotor											External medium				
													$\sigma_{\text{out}}^{\perp}$	$\mu_{\text{out}}^{\perp}$		
T (°C)	σ_1	μ_1	σ_2	μ_2	e_1/e_2	$\sigma_{\text{in}}^{\perp}$	$\mu_{\text{in}}^{\perp}$	$\sigma_{\text{in}}^{\parallel}$	$\mu_{\text{in}}^{\parallel}$	σ_{in}	μ_{in}	Material	$\sigma_{\text{out}}^{\parallel}$	$\sigma_{\text{out}}^{\parallel}$	φ_σ	φ_μ
	Cu$^{(\perp)}$		Ka$^{(\parallel)}$													
20	63	1	5×10^{-22}	1	30	61.2	1	1.6×10^{-20}	1	4×10^{21}	0	Ga	3.86	1	0.06	1
100	47	1	2.5×10^{-19}	1	30	45.6	1	7.8×10^{-18}	1	5.9×10^{18}	0	Na	10.6	1	0.23	1
	Fe$^{(\perp)}$		Sn$^{(\parallel)}$													
20	10.2	5×10^3	9.9	1	10	10.2	4.5×10^3	10.2	11	7.5×10^{-5}	413	Ga	3.86	1	0.38	2.2×10^{-4}
100	6.9	5×10^3	7.2	1	10	6.9	4.5×10^3	7	11	1.7×10^{-4}	413	Na	10.6	1	1.53	2.2×10^{-4}
	μm$^{(\perp)}$		Sn$^{(\parallel)}$													
20	2.1	1.5×10^5	9.9	1	10	2.8	1.4×10^5	2.2	11	0.24	1.2×10^4	Ga	3.86	1	1.4	7.3×10^{-6}
100	1.35	1.5×10^5	7.2	1	10	1.9	1.4×10^5	1.5	11	0.29	1.2×10^4	Na	10.6	1	5.6	7.3×10^{-6}

The same formulas (J4) and (J7) are also applicable to electrical conductivity instead of magnetic permeability, leading to

$$\sigma^{\perp} = \frac{e_1\sigma_1 + e_2\sigma_2}{e_1 + e_2}, \quad (\sigma^{\parallel})^{-1} = \frac{e_1\sigma_1^{-1} + e_2\sigma_2^{-1}}{e_1 + e_2}. \tag{J8}$$

Taking a rotor with m spiral slits of thickness e_2, at radius r we have $e_1/e_2 = \frac{2\pi r}{me_2} - 1$, where e_1 is the distance between two slits. Denoting $\overline{e_1/e_2}$ the average of e_1/e_2 over r, we have $\overline{e_1/e_2} = \pi(r_{\max} + r_{\min})/me_2 - 1$. For an anisotropic electrical conductivity rotor similar to Fury's dynamo experiment, $m = 20$ kapton sheets of thickness $e_2 = 0.33$ mm, and $15 \leqslant r \leqslant 50$ mm, leads to $\overline{e_1/e_2} \approx 30$. For an

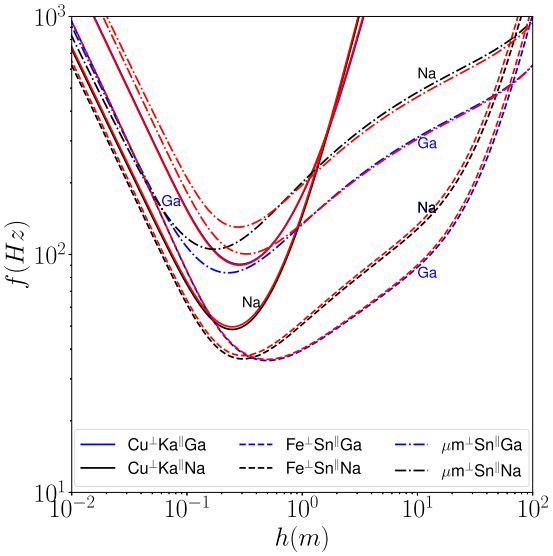

FIG. 8. The red curves calculated with the parameters in Table IV are superimposed on the curves taken from Fig. 3.

anisotropic magnetic permeability rotor, again $m = 20$ and $15 \leqslant r \leqslant 50$ mm, but taking $e_2 = 1$ mm for tin, leads to $\overline{e_1/e_2} \approx 10$. In Table IV, the values of $\sigma_{\text{in}}^{\perp}$, $\mu_{\text{in}}^{\perp}$, $\sigma_{\text{in}}^{\parallel}$, $\mu_{\text{in}}^{\parallel}$, σ_{in}, μ_{in}, φ_σ, and φ_μ have been recalculated. With these new values, the critical rotor's frequency f is plotted versus the magnetic wavelength h in Fig. 8. The difference is less than 3% for a copper/kapton or an iron/tin rotor. The difference is more significant, up to 65% for a μ-metal/tin rotor.

[1] F. Rincon, Dynamo theories, J. Plasma Phys. **85**, 205850401 (2019).

[2] S. Tobias, The turbulent dynamo, J. Fluid Mech. **912**, P1 (2021).

[3] M. Landeau, A. Fournier, H. Nataf, D. Cébron, and N. Schaeffer, Sustaining earth's magnetic dynamo, Nat. Rev. Earth Environ. **3**, 255 (2022).

[4] A. Gailitis, O. Lielausis, E. Platacis, S. Dement'ev, A. Cifersons, G. Gerbeth, T. Gundrum, F. Stefani, M. Christen, and G. Will, Magnetic field saturation in the Riga dynamo experiment, Phys. Rev. Lett. **86**, 3024 (2001).

[5] R. Stieglitz and U. Müller, Experimental demonstration of a homogeneous two-scale dynamo, Phys. Fluids **13**, 561 (2001).

[6] R. Monchaux, M. Berhanu, M. Bourgoin, M. Moulin, P. Odier, J.-F. Pinton, R. Volk, S. Fauve, N. Mordant, F. Pétrélis, A. Chiffaudel, F. Daviaud, B. Dubrulle, C. Gasquet, L. Marié, and F. Ravelet, Generation of a magnetic field by dynamo action in a turbulent flow of liquid sodium, Phys. Rev. Lett. **98**, 044502 (2007).

[7] F. J. Lowes and I. Wilkinson, Geomagnetic dynamo: A laboratory model, Nature (London) **198**, 1158 (1963).

[8] F. J. Lowes and I. Wilkinson, Geomagnetic dynamo: An improved laboratory model, Nature (London) **219**, 717 (1968).

[9] R. Avalos-Zúñiga, J. Priede, and C. Bello-Morales, A homopolar disc dynamo experiment with liquid metal contacts, Magnetohydrodynamics **53**, 341 (2017).

[10] R. Avalos-Zúñiga and J. Priede, Realization of Bullard's disc dynamo, Proc. R. Soc. A **479**, 20220740 (2023).

[11] E. Bullard, The stability of a homopolar dynamo, Math. Proc. Cambridge Philos. Soc. **51**, 744 (1955).

[12] T. Alboussière, F. Plunian, and M. Moulin, Fury: An experimental dynamo with anisotropic electrical conductivity, Proc. R. Soc. A **478**, 20220374 (2022).

[13] F. Ravelet, M. Berhanu, R. Monchaux, S. Aumaitre, A. Chiffaudel, F. Daviaud, B. Dubrulle, M. Bourgoin, P. Odier, N. Plihon, J.-F. Pinton, R. Volk, S. Fauve, N. Mordant, and F. Pétrélis, Chaotic dynamos generated by a turbulent flow of liquid sodium, Phys. Rev. Lett. **101**, 074502 (2008).

[14] T. Alboussière, K. Drif, and F. Plunian, Dynamo action in sliding plates of anisotropic electrical conductivity, Phys. Rev. E **101**, 033107 (2020).

[15] F. Plunian and T. Alboussière, Axisymmetric dynamo action is possible with anisotropic conductivity, Phys. Rev. Res. **2**, 013321 (2020).

[16] F. Plunian and T. Alboussière, Axisymmetric dynamo action produced by differential rotation, with anisotropic electrical conductivity and anisotropic magnetic permeability, J. Plasma Phys. **87**, 905870110 (2021).

[17] M. S. Ruderman and A. A. Ruzmaikin, Magnetic field generation in an anisotropically conducting fluid, Geophys. Astrophys. Fluid Dyn. **28**, 77 (1984).

[18] F. Plunian and T. Alboussière, Fast and furious dynamo action in the anisotropic dynamo, J. Fluid Mech. **941**, A66 (2022).

[19] B. Favier and M. R. E. Proctor, Growth rate degeneracies in kinematic dynamos, Phys. Rev. E **88**, 031001(R) (2013).

[20] F. Marcotte, B. Gallet, F. Pétrélis, and C. Gissinger, Enhanced dynamo growth in nonhomogeneous conducting fluids, Phys. Rev. E **104**, 015110 (2021).

[21] D. Lathrop and C. Forest, Magnetic dynamos in the lab, Phys. Today **64**(7), 40 (2011).

[22] F. Stefani, T. Albrecht, G. Gerbeth, A. Giesecke, T. Gundrum, J. Herault, C. Nore, and C. Steglich, Towards a precession driven dynamo experiment, Magnetohydrodynamics **51**, 275 (2015).
[23] M. Abramowitz and I. A. Stegun, *Handbook of Mathematical Functions with Formulas, Graphs and Mathematical Tables* (Dover, New York, 1968).
[24] W. Gale and T. Totemeir, *Smithells Metal Reference Book*, 8th ed. (Elsevier, Amsterdam, 2004).
[25] DuPont, *DuPont Kapton: Summary of Properties* (DuPont, 2022).
[26] D. Jiles, *Introduction to Magnetism and Magnetic Materials* (Springer, New York, 1991).
[27] J. Wu and D. Chung, Combined use of magnetic and electrically conductive fillers in a polymer matrix for electromagnetic interference shielding, J. Electron. Mater. **37**, 1088 (2008).